The influence of size on the intracranial distribution of biomedical nanoparticles administered by convection-enhanced delivery in minipigs

Authors: Mahsa Amirrashedi[1,2,3*], Andreas Ingemann Jensen[4*†], Qing Tang[4], Natan Johannes Willem Straathof [4], Katharina Ravn[4], Christian G.T. Pedersen[1], Louise Langhorn[5], Frantz Rom Poulsen[6,7], Max Woolley[8], David Johnson[8], Julia Williams[8], Charlotte Kidd[8], Helge Thisgaard[1,6*†], Bo Halle[6,7*†]

Affiliations:

[1]Department of Nuclear Medicine, Odense University Hospital, Odense, 5000, Denmark.

[2]Department of Applied Mathematics and Computer Science, Technical University of Denmark, Kgs. Lyngby, 2800, Denmark

[3]Danish Research Centre for Magnetic Resonance, Centre for Functional and Diagnostic Imaging and Research, Copenhagen University Hospital Amager and Hvidovre, Copenhagen, 2650, Denmark

[4]The Hevesy Laboratory, Department of Health Technology, Technical University of Denmark, Roskilde, 4000, Denmark

[5]Biomedical Laboratory, University of Southern Denmark, Odense, 5000, Denmark

[6]Department of Clinical Research and BRIDGE (Brain Research - Interdisciplinary Guided Excellence), University of Southern Denmark, Odense, 5230, Denmark

[7]Department of Neurosurgery, Odense University Hospital, Odense, 5000, Denmark

[8]Renishaw Neuro Solutions Ltd (RNS), Gloucestershire, GL12 8SP, United Kingdom

*Corresponding authors. Email: maami@dtu.dk, atije@dtu.dk, helge.thisgaard@rsyd.dk, bo.halle@rsyd.dk

†Senior authors with equal contribution

Supporting information includes:

Materials and Methods

Figs. S1 to S21

Tables S1 to S2

MATERIALS AND METHODS

Chemicals and reagents

All reagents and solvents were bought from commercial suppliers, VWR International, Sigma-Aldrich, ABCR Chemicals, FluoroChem, or TCI Chemicals, and were used as received. Technical solvents were bought from VWR International and used as received. Isotonic HEPES Buffer Solution (iso-HEPES, pH = 7.4) was prepared by dissolving HEPES free acid (2.38 g), HEPES-Na (6.6 g) and NaCl (17.54 g) in MiliQ-H_2O (2 L). Pre-mixed, custom-prepared lipid powder (3:1:1, HSPC:Chol:DSPE-PEG$_{2k}$) was bought from Lipoid GmbH. DSPE-PEG$_{1k}$-DOTA was purchased from Xi'an Ruixi Biological Technology Co., Ltd. China (Catalogue number: R-0225). TA-DOTA was purchased from CheMatech Macrocycle Design Technologies, France (Catalogue number: C128). HAuCl$_4$ 3H$_2$O was bought from Sigma-Aldrich (> 99.9%, CAS: 16961-25-4, Prod. No.: 520918). Copper-64 chloride ([^{64}Cu]CuCl$_2$) was produced on-site at the Hevesy Laboratory (0.3 - 1.5 GBq, copper-64(^{64}Cu) radionuclidic purity >99.9%, molar activity (M_A) > 1 TBq/μmol).

Equipment and analysis

The hydrodynamic diameter (Ø) and zeta potential (ζ) of the prepared nanoparticles (NPs) were measured by dynamic light scattering (DLS) on a NanoBrook ZetaPALS (Brookhaven Instruments Limited, USA). Unless stated otherwise, Ø and ζ analysis were performed at 0.1 mg/mL NP concentration in isotonic HEPES buffer (150 mM NaCl, 10 mM HEPES, pH = 7.4) at 25 °C and were done in quintuplets. Osmolarity was measured on a Gonotec Osmomat 010/030-D (Gonotec Gmbh, Germany). Radio High-Performance Liquid Chromatography (Radio-HPLC) was performed on a Hitachi Chromaster equipped with a Hitachi 5160 manual purge quaternary gradient pump, coupled to a Hitachi 5260 thermostat loop autosampler, a Hitachi 5310 column oven, a Hitachi 5430 Ultraviolet-Visible Spectroscopy (UV-Vis) multichannel detector and a radio-detector (gamma) with analog output and ca. 0.2-minute signal delay. Unless stated otherwise, routine HPLC analysis was performed using a Luna C18(2) (Ø = 2.5 μm, 100 Å) column using a 20-minute program with a 0 - 100 H$_2$O/MeCN + 0.1% TFA gradient. Routine quantification of radioactivity was performed on a Capintec CRC-55tR dose calibrator (DoseCall) and reported in Becquerel (Bq). If applicable, liquid scintillation counting (LSC) measurements were performed on a HIDEX 425-034 LSC for routine analysis or on a HIDEX 300-SL LSC for large batch analysis and reported in Bq or counts per minute (cpm). Radio Thin-Layer Chromatography (Radio-TLC) analysis was performed with a PerkinElmer Cyclone Plus phosphor imager on commercially TLC pre-coated aluminum sheets (4 × 10 cm, Merck Silica gel 60), and unless stated otherwise, run in 10% MeOH in DCM. Free ^{64}Cu could be quantified as ^{64}Cu-EDTA (Rf = 0.7) by adding EDTA to the reaction mixture prior to analysis. Radiochemical conversion (RCC) is always based on the relative converted substance, judged by Radio-TLC. Radiochemical yield (RCY) is based on the collected activity of the radiolabeled product, judged by DoseCall or LSC, and (if stated) decay corrected. Metal content (ICP) was performed on an Inductively Coupled Plasma - Optical Emission Spectroscopy (ICP-OES) iCAP 7000 Plus Series (Thermo Fisher Scientific), using the relevant reference metal standard curve, prepared with metal-free 1% HCl in H$_2$O. Size exclusion purification was performed on DP-10 (PD MidiTrap™ G-25 columns contain Sephadex G-25 resin) bought from Cytiva Sweden, using the relevant buffer (e.g., PBS (pH = 7.4) or HEPES (pH = 7.4)) at 25 °C in MiliQ-H$_2$O(18.2 MΩ·cm).

Synthesis of small citrate-stabilized gold nanoparticles, AuNP(8)

Small AuNPs were synthesized as a previously published procedure [1]. To remove residual metal, all glassware and magnets were cleaned with aqua regia (65% HNO3 in H2O/37% HCl in H2O, 1:3, v/v). To a 100 mL round bottom-flask glass containing a stirring bar was added an aq. trisodium citrate solution (74 mg in 7.5 mL H_2O, 0.25 mmol). This was then mixed with metal-free water (30 mL), aq. potassium carbonate (5.3 mg in 0.25 mL H_2O, 38 μmol) and aq. tannic acid (128 μg in 30 μL H_2O, 75 nmol). The resulting solution was then stirred while heated to 70 °C. Then aq. $HAuCl_4$ 3 H_2O (2.57 mg in 0.25 mL, 6.25 μmol) was added, resulting in a grey color and a gradual change to light red. The mixture was stirred at 70 °C for 15 minutes and then allowed to cool down to room temperature, furnishing small, citrate-stabilized AuNPs (seed solution concentration:0.032 mg/mL) (**AuNP(8)**).

Synthesis of medium citrate-stabilized gold nanoparticles, AuNP(40)

Medium-sized AuNPs were synthesized using a previously published procedure [1,2]. All glass was cleaned with *aqua regia* (65% HNO_3 in H_2O/37% HCl in H_2O, 1:3, v/v) to remove any residual metal contaminations. In a glass 100 mL round bottom flask, with a stirring bar (also cleaned with *aqua regia*), was added $HAuCl_4$ 3 H_2O (7.4 mg, 18 μmol) in MiliQ-H_2O (50 mL). The mixture was then heated up to 75 °C, and stirred vigorously, followed by the addition of an aqueous trisodium citrate solution (48.5 mg in 4 mL H_2O, 165 μmol, pH = 7), and then stirred for 1 hour at 75 °C. The resulting *dark red* suspension was then heated up to 85 °C for 30 minutes and then allowed to cool down to room temperature, furnishing the medium, citrate-stabilized AuNPs in H_2O (seed solution concentration:0.066 mg/mL) (**AuNP(40)**).

Synthesis of ^{64}Cu-DOTA-TA complex

To an acid-washed 10 mL glass vial containing dry [^{64}Cu]CuCl$_2$ (0.1 − 1 GBq) was added a stirring bar and aq. NH$_4$OAc (1.12 mg, 0.5 mL, pH = 6.8). The vial was sealed, heated up to 40 °C, and stirred for 10 minutes. To this stirring mixture was added aq. DOTA-TA (2,2',2"-(10-(2-((2-(5-(1,2-dithiolan-3-yl)pentanamido)ethyl)amino)-2-oxoethyl)-1,4,7,10-tetraazacyclododecane-1,4,7-triyl) triacetic acid) stock solution (3.2 mg, 10 μL). The pH was measured using a pH indicator (pH = 6). The mixture was then stirred for 20 minutes at 40 °C. Hereafter, an aliquot was taken from the reaction mixture and analyzed with radio-TLC, with elution in (5% NH$_4$OAc in H$_2$O: MeOH, 1:1, v/v) (RCC$_1$). The resulting ^{64}Cu-DOTA-TA in aq. NH$_4$OAc was used directly in the following steps.

Radiolabeling of AuNPs with ^{64}Cu-DOTA-TA (^{64}Cu-AuNPs)

Prior to use, all glass was cleaned with *aqua regia* (65% HNO$_3$ in H$_2$O/37% HCl in H$_2$O, 1:3, v/v) to remove any residual metal contaminations. To a 50 mL glass round-bottom flask equipped with a stirring bar, AuNPs dispersion was added (20 mL). To this was added ^{64}Cu-DOTA-TA complex, prepared as described above (1 mL, 1100 MBq), transferring all the activity into the reaction vial containing the AuNPs (A$_{trans}$ > 95%). Then, the mixture was stirred for 20 minutes at room temperature. Hereafter, an aliquot was taken and analyzed by radio-TLC (5% NH$_4$OAc in H$_2$O:MeOH, 1:1, v/v) (RCC$_2$) to confirm the successful attachment of the ^{64}Cu-DOTA-TA to the AuNPs. Following this, the surface of the AuNPs was further decorated by adding a freshly prepared aqueous solution of MeO-PEG$_{2K}$-SH (2.1 mg, 100 μL), and the mixture was stirred for 15 minutes at room temperature. Hereafter, an aliquot was taken and analyzed by radio-TLC (5% NH$_4$OAc in H$_2$O:MeOH, 1:1, v/v) (RCC$_3$) to confirm the continued surface attachment of the ^{64}Cu-DOTA-TA. A size-exclusion column (Cytiva PD MiniTrap G-25) was equilibrated with saline (5

119 mL) prior to sample application. A dispersion of ^{64}Cu-AuNPs in saline (100 μL) was applied to
120 the column and then eluted with saline, and fractions (14 fractions of 200 μL, depending on loading
121 and column size) were collected. Once all the fractions were collected, they were analyzed for
122 activity. The mixture was transferred into a centrifugation filter (MWCO = 30 kDa) and spun to
123 remove the aqueous buffer (4400 rpm). Hereafter, the ^{64}Cu-AuNPs were redispersed in sterile
124 saline (15 mL), and the filter cartridge was centrifuged again to remove the saline (4400 rpm). The
125 purified ^{64}Cu-AuNPs were resuspended in sterile saline (6 mL) and transferred into a 20 mL glass
126 vial. The activity of the vial was measured (RCY_1), and an aliquot (1 mL) was immediately
127 removed for analysis by DLS and Size-Exclusion Chromatography (SEC) (**table S2**). The
128 remaining ^{64}Cu-AuNPs dispersion (5 mL) was then sterile filtered (Acrodisc syringe filter, Ø = 13
129 mm, 0.2 μm) into a sterile septum-sealed 10 mL vial, which afforded the final product ^{64}Cu-AuNPs
130 (RCY_2).

Preparation of DOTA-LIPs

131
132 In a 10 mL metal-free vial, was added pre-mixed lipid powder HSPC:Chol:DSPE-PEG$_{2k}$ (44 mg,
133 59.4 μmol, 3:1:1, mass ratio), then DSPE-PEG$_{1k}$-DOTA (1.28 mg, 6 μmol) were added to reach 1
134 mol% of DOTA in the resulting lipid mixture. t-BuOH:H$_2$O (3 mL, 9:1, v/v) was added and the
135 solids were dissolved by sonication. The resulting solution was aliquoted into three vials separately
136 (1 mL each) and freeze-dried. The obtained lyophilizate was hydrated with metal-free iso-HEPES
137 (1 mL) buffer at 65 °C, followed by manual extrusion in an Avanti mini extruder with a 100 nm
138 filter. The resulting LIPs are in the following referred to as DOTA-LIPs. Hereafter, the lipid
139 dispersion was transferred to a glass vial and stored in the refrigerator for further use and analysis.

Preparation of ^{64}Cu-DOTA-LIPs, ^{64}Cu-LIP(130)

140
141 To a metal-free vial containing dry [^{64}Cu]CuCl$_2$ (360 MBq), DOTA-LIPs (20 mM lipid, 750 μL,
142 **table S1**) were added. The reaction mixture was magnetically stirred at 55 °C for 2 hours. After
143 this, 1 μL of the reaction solution was aliquoted and mixed with EDTA in iso-HEPES (100 μL, 20
144 nmol) and analyzed by radio-TLC (5% NH$_4$OAc in H$_2$O:MeOH, 1:1, v/v) (RCC_1). After 30
145 minutes, EDTA (50 μL) was added to the entire reaction mixture, stirred for 10 minutes while
146 cooling to room temperature and analyzed by radio-TLC (RCC_2). The ^{64}Cu-LIPs were then
147 purified by elution through a PD-10 size-exclusion column. The final product was then passed
148 through a sterilized Millex-HV 0.45 μm filter. An aliquot of the product (1 mL) was removed for
149 analysis, including radio-TLC (RCC_3), DLS and ICP-OES. In this study, the preparation of ^{64}Cu-
150 DOTA-LIPs was conducted three times (Batch # 5 to 7) with minor variations. Further elaboration
151 on the experimental details can be found in **table S1** and **table S2**.

Characterization of ^{64}Cu-AuNPs and ^{64}Cu-DOTA-LIPs

152
153 Total activity was measured by dose-calibrator, and purity was determined radio-TLC using a
154 mixture of (5 % NH4OAc in H$_2$O:MeOH, 1:1, v/v). Size (Ø) and polydispersity index (PDI) were
155 determined by DLS, UV-Vis, and transmission electron microscopy (TEM) analysis. ICP-OES
156 was used to determine the gold (Au) and phosphorus (P) concentrations using predetermined
157 standards (**table S2**). The numbers of LIPs (*n.LIPs*) and AuNPs (*n.AuNPs*) in the final product
158 were calculated using the following equations, adapted from the literature [3].

159

160
$$n.LIPs = 17.69 \times \left\{ \left(\frac{\text{Ø}_{vol-DLS}}{2} \right)^2 + \left(\frac{\text{Ø}_{vol-DLS}}{2} - 5 \right)^2 \right\}$$

161

162 In the below equation, m is the mass of each AuNP, and c is the Au concentration as judged by
163 ICP-EOS analysis.

164

165 $$m = \left(\frac{4}{3}\right) \times \pi \times \left(\frac{\text{Ø}_{vol-DLS}}{2}\right)^3 \times 19.30$$

166 $$n.AuNPs = \frac{m}{(c \times 10^{-18})}$$

167

168

Stability and size-exclusion analysis

170 A size-exclusion column (Cytvia PD MiniTrap G-25) was equilibrated with saline (5 mL) prior to
171 sample application. A dispersion of the ^{64}Cu-DOTA-LIPs in iso-HEPES (200 µL) was applied
172 onto the column and then eluted with iso-HEPES, and fractions (14 fractions of 200 µL) were
173 collected. Subsequently, the fractions were subjected to activity analysis using a dose calibrator.

174 In the case of AuNPs, the following general procedure was followed. A size-exclusion column
175 (Cytvia PD MiniTrap G-25) was equilibrated with saline (5 mL) prior to sample application. A
176 dispersion of the AuNPs in saline (100 µL) was applied onto the column and then eluted with
177 saline, and fractions (14 fractions of 200 µL, depending on loading and column size) were
178 collected. After collecting all fractions, they were analyzed for activity, containing the purified
179 NPs.

Transmission Electron Microscopy of AuNPs.

181 From the final AuNPs solution (vide infra), 5 µl were placed on freshly glow discharged formvar
182 coated 200 mesh nickel TEM grids (EMS Diasum) and allowed to adsorb for 1 minute, after which
183 excess solution was removed using filter paper. Samples were imaged using a Tecnai T12 Biotwin
184 (Thermo Fisher) equipped with a Gatan Orius CCD camera. The resulting pictures are displayed
185 shown in **fig. S13**.

Animals and housing

187 Three Göttingen female-minipigs (Ellegaard Göttingen Minipigs A/S, Dalmose, Denmark)
188 weighing on average 9.3 ± 0.18 kg (ranging from 8.9 to 9.6 kg) and approximately two months old
189 were included in the present study. Minipigs were used due to their slow growth rate, making them
190 optimal for long-term CED studies. Prior to the initiation of experimental procedures, the animals
191 were allowed to acclimatize for one month at the animal facility of the Biomedical Laboratory,
192 University of Southern Denmark. The animals were kept in communal enclosures with sawdust
193 bedding and fed twice daily with a standard minipig diet (Altromin 9069, Altromin, Germany) and
194 free access to water. Enrichment was provided in the form of hay, toys, and daily human
195 interaction. The animals were attended to at least twice daily and monitored for general well-being,
196 physical activity, and food consumption. Body weight was monitored weekly.

Anesthesia, analgesia, and perioperative procedures

For all surgical and imaging procedures, minipigs were premedicated in a calm environment with an intramuscular injection of medetomidine 0,03 mg/kg (Cepetor Vet., 10 mg/mL, ScanVet Animal Health, Fredensborg, Denmark), midazolam 0,25 mg/kg (Midazolam 5 mg/mL, hameln pharma GmbH, Hameln, Germany), ketamine 5 mg/kg (Ketaminol Vet., 100 mg/mL, MSD Animal Health, Copenhagen, Denmark) and butorphanol 0,2 mg/kg (Butomidor Vet. 10 mg/mL, Salfarm Danmark A/S, Kolding, Denmark). Two Intravenous(IV) accesses and a urinary catheter size six were placed before general anesthesia (GA) was induced with propofol (Propomitor Vet., 10 mg/mL, Orion Pharma Animal Health, Copenhagen, Denmark), and the pig was intubated with a cuffed orotracheal tube size 5,5. For surgical procedures, the animal was moved to the operating table and GA was maintained by a constant rate infusion of propofol 10 mg/kg/h and fentanyl 20 μg/kg/h while being mechanically ventilated with a tidal volume of 7-8 mL/kg and a respiratory frequency of 22-26 per minute. During surgical procedures, non-invasive blood pressure, electrocardiogram, body temperature, heart rate, oxygen saturation, and capnography were continuously monitored. To prevent postoperative pain, minipigs were administered an intramuscular injection of meloxicam 0,4 mg/kg (Metacam 5 mg/mL, Boehringer Ingelheim Vetmedica GmbH, Ingelheim/Rhein, Germany) on the day of surgery. For antibiotic prophylaxis, an IV infusion of Cefuroxime 375 mg (Cefuroxime 'Fresenius Kabi,' 750 mg, Fresenius Kabi AB, Uppsala, Sweden) was administered preoperatively in combination with an intramuscular injection of Amoxicillin 20 mg/kg (Noromox Prolongatum Vet., 150 mg/ml, ScanVet Animal Health, Fredensborg, Denmark). For imaging procedures, the anesthetized animal was transported to the imaging facility while maintaining anesthesia with propofol 2 mg/kg/h and manually ventilating the animal using a hand-held infant resuscitator (Ambu® SPUR II, Ambu A/S, Ballerup, Denmark) with a constant oxygen supply. During transport, heart rate and peripheral oxygen saturation (SpO_2) were continuously monitored with pulse oximetry, and rectal body temperature was regularly monitored. During all imaging sessions, minipigs were mechanically ventilated, and GA was maintained during surgical procedures. Hypothermia was prevented during all procedures using heated blankets and heated infusion bags.

Head immobilization and pre-catheter implantation MRI

A dedicated MRI-compatible head frame (Renishaw Neuro Solutions Ltd, Wotton-Under-Edge, Gloucestershire, UK) [4, 5] was fixed on the anesthetized animal using two zygomatic screws, a moldable palate tray, and a snout strap to fully immobilize the head. A fiducial arc was attached onto the frame and the animal was transferred in the prone position to the scanner bed of a GE SIGNA PET/MRI scanner with a magnetic field strength of 3 T (GE Healthcare, Waukesha, WI, USA). The upper anterior array (UAA) coil was attached around the fiducial arc. The step-by-step overview of all procedures on the surgery day is summarized in (**Fig. 5**). 3D MRI scans consisting of T1-weighted BRAVO (Repetition time = 8.8 ms, Echo time = 3.45 ms, Inversion time = 450 ms, Number of averages = 3, Flip angle= 12, Matrix size = 256 × 256 × 150, in-plane resolution = 0.8 mm × 0.8 mm, Slice thickness = 0.8 mm) and T2-weighted (Repetition time = 2742 ms, Echo time = 139.16 ms, Inversion time = 450 ms, Number of averages = 2, Flip angle = 12, Matrix size = 512 × 512 × 200, in-plane resolution = 0.39 mm × 0.39 mm, Slice thickness = 0.6 mm) sequences were obtained. For preoperative MRI acquisition, an Upper Anterior Array (UAA) providing a superior-inferior (S/I) coverage of 54 cm and right-left (R/L) coverage of 50 cm was employed due to limitations with fitting the head frame within the brain coil. The preoperative MRI scans were then loaded into the neurosurgical planning software Neuroinspire™ (Renishaw Neuro

242 Solutions Ltd, Wotton-under-Edge, Gloucestershire, UK) to plan the implantation trajectories of
243 two neuroinfuse™ CED catheters within the putaminal targets connected to an implanted
244 transcutaneous port (Renishaw Neuro Solutions Ltd, Wotton-Under-Edge, Gloucestershire, UK),
245 as illustrated in (**fig. S14, A**). Immediately after surgery, 22 µL of a mixture of Gd (Gadovist
246 1mmol/mL, Bayer Healthcare, Germany) and sterile artificial cerebrospinal fluid (aCSF, Torbay
247 Pharmaceutical Manufacturing Unit, Paignton, UK) in a concentration of 2mM Gd were infused
248 through the reaccess port into the implanted catheters. Subsequently, a T1-weighted MRI was
249 performed to confirm the targeting accuracy and verify proper catheter placement. For
250 postoperative MRI scans, an 8-channel high-resolution brain array was utilized.

Ethical approval

252 All animal procedures were conducted per the approval from the Danish Animal Experiments
253 Inspectorate (license no. 2020-15-0201-00553). The experiments were conducted according to the
254 EU directive 2010/63/EU on the protection of animals used for scientific purposes.

Implantation of neuroinfuse™ chronic drug delivery system

256 To enable CED, the Neuroinfuse™ chronic drug delivery system [6] and preclinical stereotactic
257 system (**Fig. 7, A**), developed by Renishaw Neuro Solutions Ltd, was used. Following the
258 preoperative MRI scans, the animal was transferred from the scanner unit to the operation theatre.
259 With the head still fixated in the dedicated head frame, the animal was placed in a prone position.
260 An 8-10 cm midline incision was made on the top of the skull. The periosteum was separately
261 elevated, and the device was implanted (**Fig. 7, B**). The skin incision was closed (**Fig. 7, C**) in two
262 layers with interrupted Vicryl 2-0 subcutaneously and continuous Ethilon 3-0 cutaneously. The
263 zygomatic wounds were closed with interrupted Ethilon 3-0 sutures, and an attached port
264 application infusion set.

Postoperative recovery and follow-up

266 As described above, a postoperative MRI was acquired to confirm catheter placement. After this,
267 the animal was referred to the animal facility for postoperative recovery and care. Special attention
268 was drawn towards the awakening phase to ensure the animals would avoid head traumas due to
269 anesthetic side effects. Until full recovery, animals were closely monitored. In the subsequent
270 period, animals were inspected a minimum of twice daily and assessed for neurological deficits
271 and abnormal behavior. Wounds were inspected daily for signs of infection, and the skin/bone-
272 anchored port interface was cleaned with sterile water when necessary.

Euthanasia

274 On the last day of the study, pigs were euthanized with an intravenous overdose of pentobarbital
275 100 mg/kg (Exagon Vet., 400 mg/mL, Salfarm Danmark, Kolding, Denmark) while in general
276 anesthesia.

Infusion method of radiolabeled nanoparticles

278 The administration of ^{64}Cu-NPs commenced seven days after catheter implantation by connecting
279 the application set to the transcutaneous port (**Fig. 5, B** and **fig. S14, C**). Infusions were repeated
280 through the transcutaneous port at weekly intervals for a total of four weeks. Each week, a different
281 type of NP was synthesized, loaded into fixed volume extension sets (FVES), and infused into the
282 subjects. Briefly, for each infusion, two 300 µL FVES were filled with dispersions of ^{64}Cu-NPs
283 at specific sizes. Transportation, leakage, and delivery risk of the radiolabeled infusate is addressed

284   by FVES design. Each end terminates in a modified, low dead-volume male luer connector
285   consisting of a small septum seal. Safe access to the active infusate held within is achieved through
286   the attachment of a modified female lure connector fitted with a centralized needle. One end of the
287   FVES tube was connected to the corresponding delivery channel of the 4-channel port application
288   set (only 2/4 port channels were accessed for this study), while the other end was attached to a 6 m
289   extension line, which in turn connected to standard syringes pre-filled with artificial CSF (**Fig. 6,**
290   **B**). The extension lines were utilized to allow infusions from two syringe pumps located outside
291   the MRI scanning room. Once the application set was secured to the transcutaneous bone-anchored
292   port, the infusions were initiated with 40-minute linear ramps. The infusion rate was gradually
293   increased to a maximum rate of 3 µL/min per catheter with a total volume of 600 µL of ^{64}Cu-NPs
294   delivered per infusion. The inert aCSF is used to push the active therapy through the FVES port
295   and then catheters into the desired target. An additional dead volume is added to the overall volume
296   to ensure only inert buffer is left within the implantable device between reaccess infusion periods.
297   Once the infusion was finished, the catheters were left in situ for an additional 15 minutes, and the
298   pump rate gradually decreased to stabilize the pressure before disconnecting the infusion lines.
299   The application set was then removed from the port.

300   **Positron Emission Tomography (PET)**

301   After attaching the infusion lines to the application set, the animal was positioned inside an 8-
302   channel high-resolution brain array coil providing (S/I) coverage of 24 cm and (R/L) coverage of
303   22 cm for PET/MRI studies. PET emission data were collected dynamically over a 135-minute
304   period, beginning at the start of the infusion. To facilitate quantitative analysis and to study the
305   biodistribution of ^{64}Cu-NPs at different time points, list-mode emission files were re-binned into
306   nine frames of 15 minutes each to produce dynamic PET scans and were reconstructed into a 256
307   × 256 × 89 matrix size (1.1718 mm × 1.1718 mm × 2.78 mm) using GE's Time of Flight Bayesian
308   penalized reconstruction algorithm (Q.clear) with β parameter set to 100. Quantitative corrections,
309   including detector geometry modeling, normalization, attenuation, scattering, decay, and dead
310   time were considered inside the iterative loop. Of note, an MRI-based attenuation correction
311   (MRAC) method was applied to correct attenuated annihilation photons. Additionally, we acquired
312   a single MRI scan in each session to serve as an anatomical guide for defining the Volume of
313   interests (VOIs). MRI acquisitions were performed using the same setup and protocols described
314   in the previous section. The experimental timeline is also shown in (**Fig. 5, C**).

315   **PET Data analysis**

316   Image analysis was carried out using GE's PET4D workstation, Image J, and Amide v1.0.4
317   software. Data visualization and a part of the image processing were performed in MATLAB
318   R2023a.

319   **Line profile analysis**

320   For quantitative analysis of the line profile, we computed the full-width half maximum (FWHM)
321   and full-width tenth maximum (FWTM) at different time points of the infusion. This was done by
322   fitting a Gaussian curve to the pixel intensity values along the line passing through the center of
323   the catheter and calculating the width of these profiles at 10% and 50% of the maximum value.
324   For each catheter, two lines perpendicular to the catheter trajectory were drawn on transverse and
325   sagittal planes, and the final FWHM was obtained by averaging the transverse ($FWHM_{axial}$) and
326   sagittal ($FWHM_{sagittal}$) values. The same was performed for FWTM analysis.

Iso-contour plots

We studied the anisotropy in the spatial dispersion of NPs using iso-contour plots. To this end, three consecutive cross-sectional slices with the highest uptake value surrounding the left catheter from the same animal were selected, averaged, and then normalized to the maximum value in the image. The final image matrix was resampled to a finer grid of 1024×1024, and a contour plot was generated based on the processed image using an integrated program in MATLAB. The filled contour plot represents iso-lines obtained from an image and fills the areas between these iso-lines with consistent colors that correspond to the final image matrix values.

Volume of distribution (Vd)

The distribution of the ^{64}Cu-NPs was assessed by conducting a comprehensive volumetric analysis on dynamically reconstructed PET scans. MRI images obtained in each scanning session were used as anatomical reference for accurate VOI definition. First, an MRI-guided ellipsoidal VOI encompassing the entire brain was established for each scan (the administration lines were excluded from the VOI accurately), and Vd values were then extracted from these VOIs by defining various threshold levels, ranging from 10% to 90% of the maximum uptake value within the VOI. Before inclusion in the Vd assessment, all VOIs underwent visual inspection and editing to ensure accuracy.

Time activity curve (TAC)

The activity inside the predefined VOIs at different time points was normalized to the net total activity (A_{total}) to generate normalized TAC plots. The area under the curve (AUC) was then calculated for TAC, for dynamically assessed Vds for different thresholds, and for FWHM/FWTM plots (versus time) to allow for statistical comparison among different ^{64}Cu-NPs groups.

Statistical Analysis

Data were reported as mean values ± standard error of the mean (SEM) unless otherwise mentioned. Graphs were created in MATLAB 2023a. Statistical testing was performed using GraphPad Prism software version 5 (San Diego, CA, USA). One-way analysis of variance (ANOVA) followed by Tukey's test was selected to compare the AUC results (FWHM, TAC, and Vd) among different groups of NPs with $P < 0.05$ considered significant. Significant difference was defined as $*P < 0.05$, $**P < 0.01$, $***P < 0.001$.

366 **TABLES**

367

368 **Table S1. Experimental details of ^{64}Cu-DOTA-LIPs.**

Batch number	DOTA-LIP volume	[^{64}Cu]CuCl$_2$	Reaction time (hours)	EDTA challenge	Stability analysis	ICP-OES
5	750 μL	360 MBq	2	yes	no	no
6	1000 μL	600 MBq	1.5	yes	yes	yes
7	750 μL	1100 MBq	1.5	yes	no	yes

369 Abbreviation: ^{64}Cu, copper-64; LIP, liposomes; ICP-OES, inductively coupled plasma - optical
370 emission spectroscopy.

372   **Table S2. Overview of ^{64}Cu-NPs prepared and supplied.**

Batch	1	2	3	4	5	6	7
Administered to pigs	no	no	yes	yes	no	yes	yes
Size Classification	n.a.	n.a.	Medium	Small	n.a.	Large	Large
Name	-	-	^{64}Cu-AuNP(40)	^{64}Cu-AuNP(8)	-	^{64}Cu-LIP(130)	^{64}Cu-LIP(130)
HAuCl$_4$ 3H$_2$O (µmol)	18.0	6.3	18.0	6.3	n.a.	n.a.	n.a.
PDI	0.329 ± 0.002	0.329 ± 0.018	0.319 ± 0.005	0.329 ± 0.011	0.126 ± 0.014	0.070 ± 0.043	0.059 ± 0.027
Ø$_{vol-DLS}$ (nm), NPs	17.04 ± 0.31	5.74 ± 0.23	13.37 ± 0.83	5.42 ± 0.9	60.10 ± 8.49	116.43 ± 1.88	101.32 ± 9.36
Ø$_{int-DLS}$ (nm), NPs	-	-	52.96 ± 2.74	19.38 ± 6.08	121.22 ± 4.12	123.08 ± 14.6	118.34 ± 9.36
Ø$_{num-DLS}$ (nm), NPs	-	-	12.72 ± 0.82	5.20 ± 1.01	n.a.	n.a.	n.a.
^{64}Cu activity used (GBq)	0.0863	0.0753 MBq	1.1	1.07	0.106	0.602	1.1
^{64}Cu-DOTA complex, RCC$_1$	96%	98%	97%	97%	n.a.	n.a.	n.a.
^{64}Cu -DOTA-NPs, RCC$_2$	80%	89%	70%	95%	n.a.	n.a.	n.a.
^{64}Cu-DOTA-PEG-NPs, RCC$_3$	64%	-	85%	89%	99%	98%	97%
RCY (ndc.)	-	-	62%	69%	-	67%	83%
PDI, ^{64}Cu-DOTA-PEG-NPs	-	-	0.153 ± 0.030	0.223 ± 0.009	0.196 ± 0.015	0.046 ± 0.014	0.126 ± 0.035
Ø$_{vol-DLS}$ (nm), ^{64}Cu-DOTA-PEG-NPs	25.12 ± 0.93	17.75 ± 2.33	39.84 ± 6.89	7.53 ± 0.36	85.74 ± 3.16	116.82 ± 7.37	86.61 ± 7.93
Ø$_{int-DLS}$ (nm), ^{64}Cu-DOTA-PEG-NPs	-	-	38.27 ± 7.63	6.10 ± 0.16	124.12 ± 4.12	133.83 ± 8.50	127.27 ± 9.88
Ø$_{TEM}$ (nm)	-	-	14.2 ± 1.3	4.8 ± 0.8	-	-	-
ζ(mV), ^{64}Cu -DOTA-PEG-NPs	-	-	-4.86	-9.55	-	-4.89	-2.45
λ$_{max}$ (nm), UV-Vis	-	-	540	513	n.a.	n.a.	n.a.
Ø$_{UV-Vis}$ (nm), ^{64}Cu-DOTA-PEG-NPs	-	-	68 ± 8.0	6.6 ± 0.6	n.a.	n.a.	n.a.
ICP-OES (mM)	-	-	9.14 (0.18 mg/mL)	6.09 (0.12 mg/mL)	-	3.14	2.55
Number of NPs per mL	-	-	2.78 × 10^{11}	2.32 × 10^{13}	-	6.8 × 10^{12}	6.9 × 10^{12}
^{64}Cu-NPs after sterilization, Overall RCY (ndc.)	54%	66%	43%	45%	92%	48%	45%
^{64}Cu-NPs after sterilization, Overall RCY (dc.)	69%	79%	58%	56%	-	55%	53%
Final total activity (MBq)	46.3	49.8	480	487	100	289	460
Final product volume (mL)	-	-	5	5	-	4	4
Specific Activity (ndc.)	-	-	10.50 GBq/µmol	15.99 GBq/µmol	-	23.01 GBq/µmol	45.09 GBq/µmol

373 Reported data are given as mean ± standard deviation. Abbreviations: $\varnothing_{\text{vol-DLS}}$, the volume-
374 weighted hydrodynamic diameter measured by DLS; $\varnothing_{\text{int-DLS}}$, the intensity-weighted
375 hydrodynamic diameter measured by DLS; $\varnothing_{\text{TEM}}$, the diameter of the AuNP gold core measured
376 by TEM; $\varnothing_{\text{UV/Vis}}$, the AuNP diameter corresponding to the absorption maximum; PDI,
377 polydispersity index; ζ, zeta potential; DLS, dynamic light scattering analysis; n.a., not applicable;
378 TEM, transmission electron microscopy; UV/Vis, ultraviolet-visible spectroscopy. RCY,
379 radiochemical yield; ndc., non-decay corrected; dc., decay corrected; RCC, Radio chemical
380 conversion.

381 **FIGURES**

382
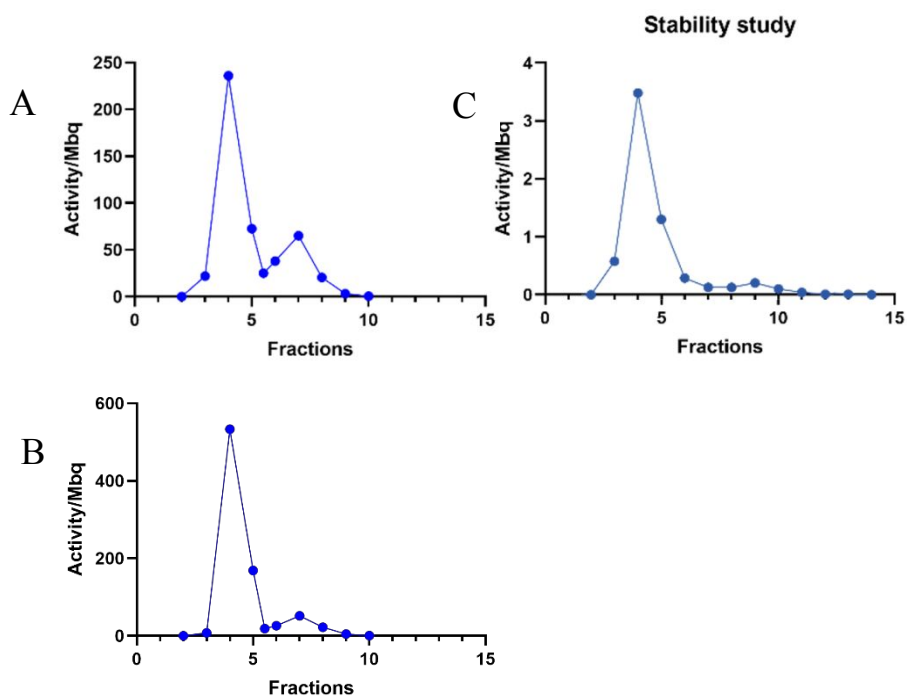
397 **Fig. S1. Size exclusion and stability of ^{64}Cu-LIP(130).** (**A**) ^{64}Cu-activity (MBq) analysis of ^{64}Cu-
398   LIPs PD-10 size exclusion fractions (Batch #6). (**B**) ^{64}Cu-activity (MBq) analysis of ^{64}Cu-
399   LIPs PD-10 size exclusion fractions (Batch #7), (no stability assay was performed for
400   Batch #7). (**C**) ^{64}Cu-activity (MBq) analysis of ^{64}Cu-LIPs PD-10 size exclusion fractions
401   after 24 hours (stability assay for Batch #6). Abbreviations: ^{64}Cu, copper-64; LIP,
402   liposome.
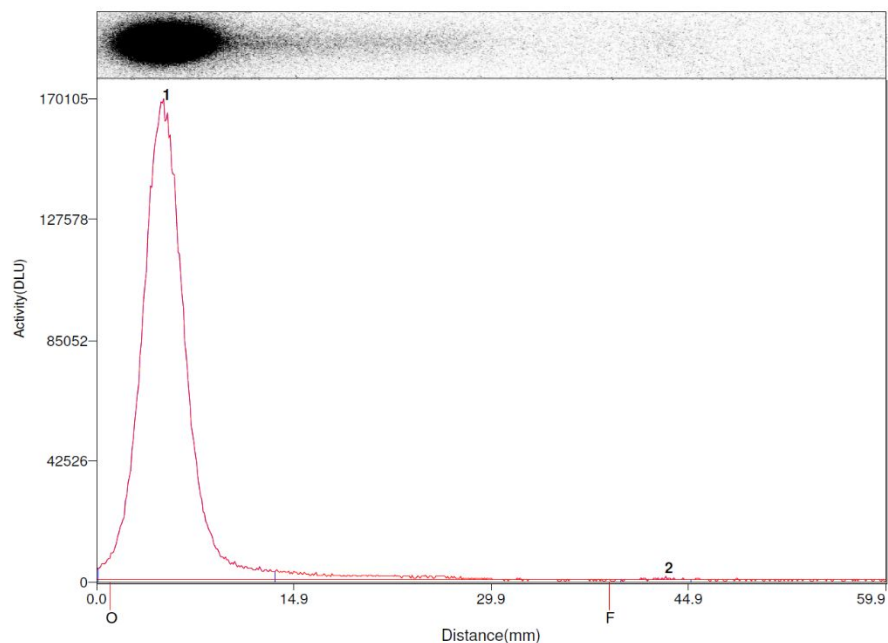
Fig. S2. Radio-TLC of ^{64}Cu-LIP(130) – Batch #5. RCC_3 = 99% (final product). Radio-TLC analysis was performed with a PerkinElmer Cyclone Plus phosphor imager on commercially TLC pre-coated aluminum sheets (4 × 10 cm, Merck Silica gel 60), using an eluent-mix (5% NH$_4$OAc in H$_2$O:MeOH, 1:1, v/v). Free ^{64}Cu could be quantified as ^{64}Cu-EDTA (Rf = 0.7) by adding EDTA to the reaction mixture prior to analysis. Abbreviations: RCC, Radio chemical conversion; ^{64}Cu, copper-64; LIP, liposome.

435
436
437
438
439
440
441
442
443
444
445
446
447
448
449
450
451
452
453
454
455
456
457
458
459
460
461
462
463
464
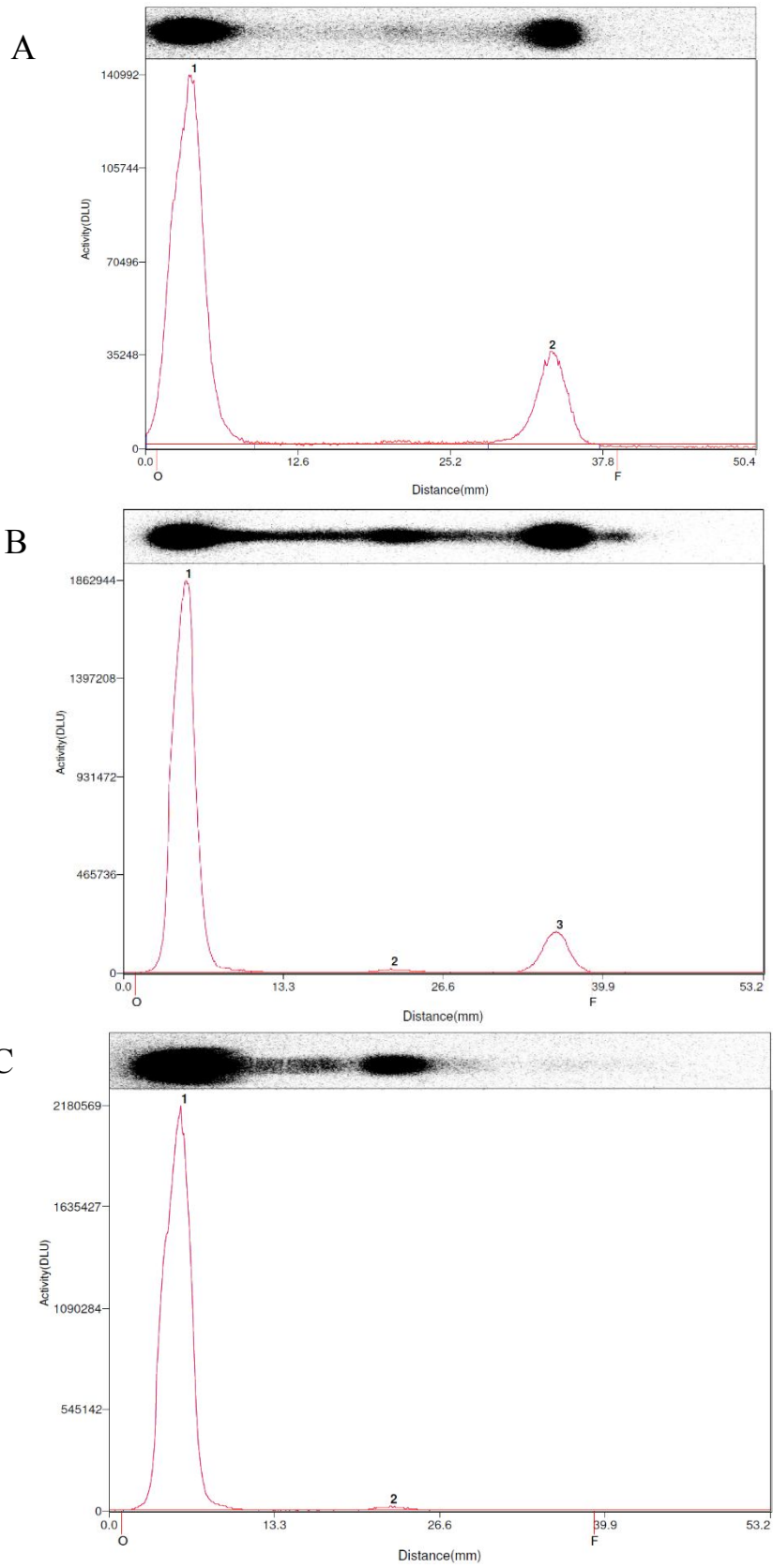
Fig. S3. Radio-TLC of ^{64}Cu-LIP(130) – Batch #6. (A) RCC_1 = 82% (1 hour), **(B)** RCC_2 = 91% (1.5 hour), **(C)** RCC_3 = 98% (final product). Radio-TLC analysis was performed with a PerkinElmer Cyclone Plus phosphor imager on commercially TLC pre-coated aluminum sheets (4 × 10 cm, Merck Silica gel 60), using an eluent-mix (5% NH_4OAc in H_2O:MeOH, 1:1, v/v). Free ^{64}Cu could be quantified as ^{64}Cu-EDTA (Rf = 0.7) by adding EDTA to the reaction mixture prior to analysis. Abbreviations: RCC, Radio chemical conversion; ^{64}Cu, copper-64; LIP, liposome.

Fig. S4. Radio-TLC of ⁶⁴Cu-LIP(130) – Batch #7. (A) RCC_1 = 84% (1 hour), **(B)** RCC_2 = 89% (1.5 hour), **(C)** RCC_3 = 97% (final product). Radio-TLC analysis was performed with a PerkinElmer Cyclone Plus phosphor imager on commercially TLC pre-coated aluminum

506 sheets (4 × 10 cm, Merck Silica gel 60), using an eluent-mix (5% NH_4OAc in H_2O:MeOH,
507 1:1, v/v). Free ^{64}Cu could be quantified as ^{64}Cu-EDTA complex (Rf = 0.7) by adding EDTA
508 to the reaction mixture prior to analysis. Abbreviations: RCC, Radio chemical conversion;
509 ^{64}Cu, copper-64; LIP, liposome.

510

511

512
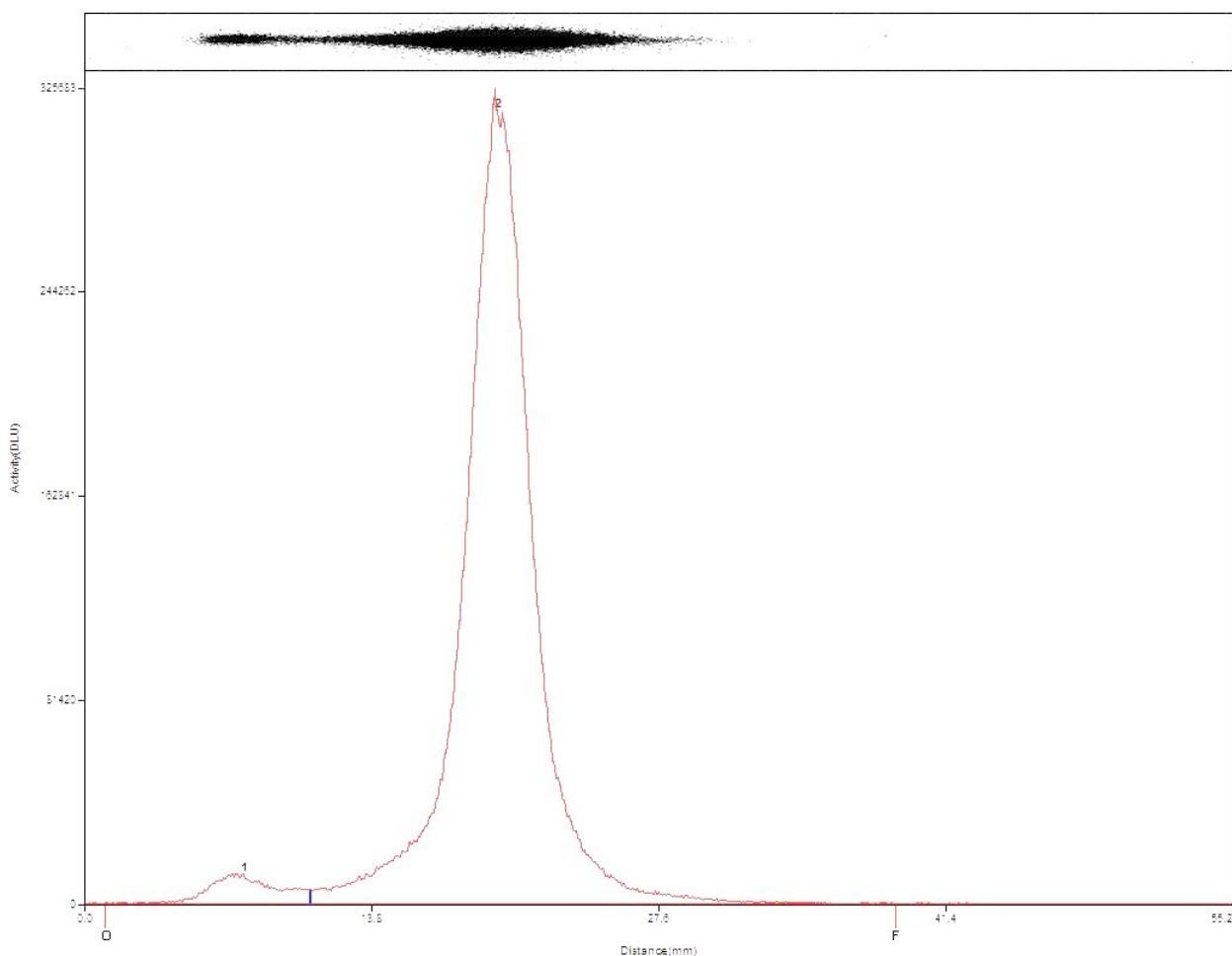
513 **Fig. S5. Radio-TLC of ^{64}Cu-DOTA-TA complex – Batch #1.** RCC_1 = 97%. The complex was
514   prepared using the standard method of 5 nmol DOTA and 100 MBq [^{64}Cu]CuCl$_2$. Radio-
515   TLC analysis was performed with a PerkinElmer Cyclone Plus phosphor imager on
516   commercially TLC pre-coated aluminum sheets (4 × 10 cm, Merck Silica gel 60), using an
517   eluent-mix (5% NH$_4$OAc in H$_2$O:MeOH, 1:1, v/v). Free ^{64}Cu could be quantified as ^{64}Cu-
518   EDTA complex (Rf = 0.7) by adding EDTA to the reaction mixture prior to analysis.
519   Abbreviations: RCC, Radio chemical conversion; ^{64}Cu, copper-64.

520

521

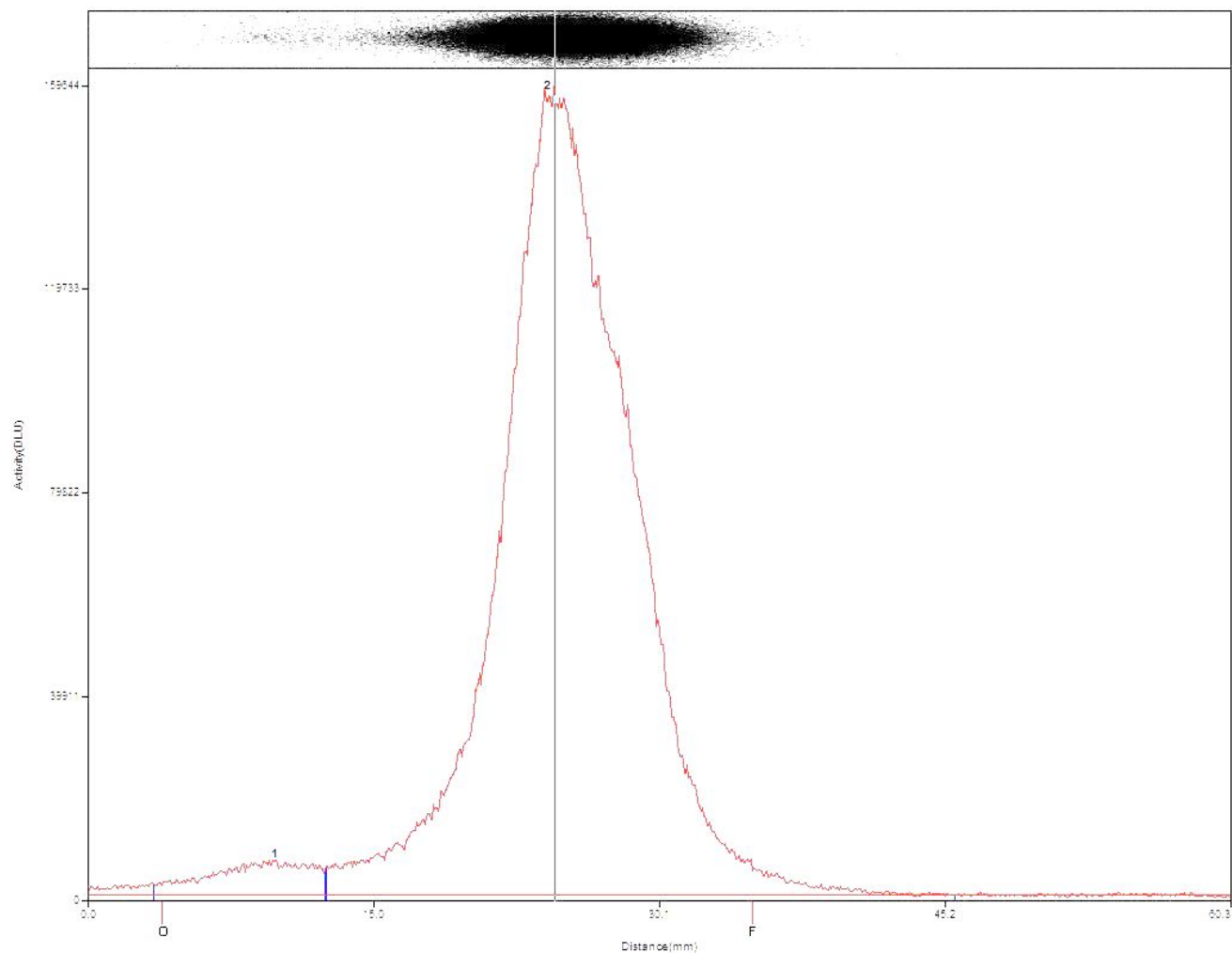**523**

524
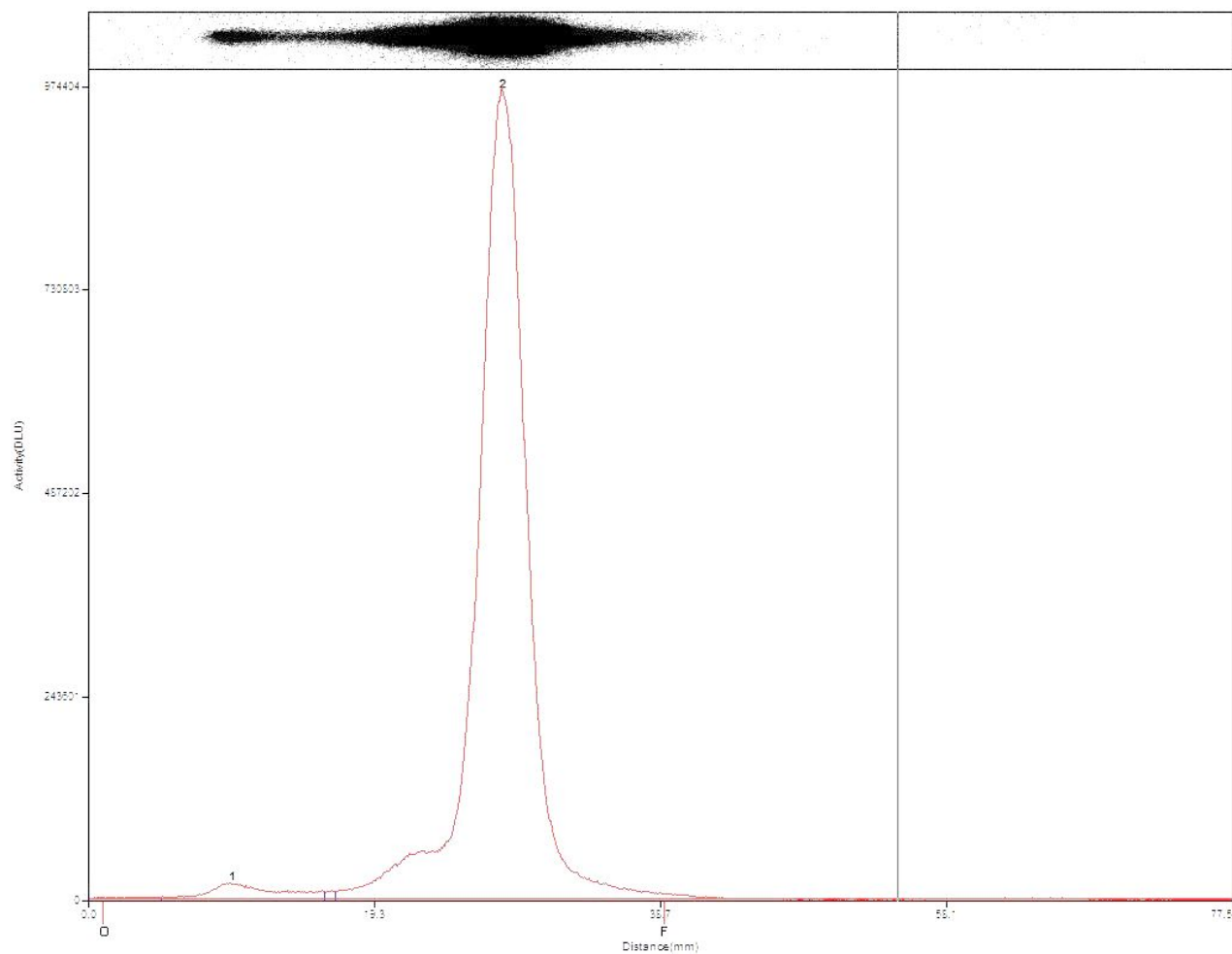
Fig. S6. Radio-TLC of ^{64}Cu-DOTA-TA complex – Batch #2. RCC_1 = 98%. Complex prepared using the standard method using 5 nmol DOTA, 1 GBq [^{64}Cu]CuCl$_2$. Radio-TLC analysis was performed with a PerkinElmer Cyclone Plus phosphor imager on commercially TLC pre-coated aluminum sheets (4 × 10 cm, Merck Silica gel 60), using an eluent-mix (5% NH$_4$OAc in H$_2$O:MeOH, 1:1). Free ^{64}Cu could be quantified as ^{64}Cu-EDTA complex (Rf = 0.7), by adding EDTA to the reaction mixture prior to analysis. Abbreviations: RCC, Radio chemical conversion; ^{64}Cu, copper-64.

532

**Fig. S7. Radio-TLC of ^{64}Cu-DOTA-TA complex – Batch #3.** RCC_1 = 97%. The complex was prepared using the standard method of 6.2 nM DOTA, 1 GBq [^{64}Cu]CuCl$_2$. Note: peak broadening is likely to occur after prolonged exposure, leading to polymer degradation and de-sulfidation of the DOTA linkers. Radio-TLC analysis was performed with a PerkinElmer Cyclone Plus phosphor imager on commercially TLC pre-coated aluminum sheets (4 × 10 cm, Merck Silica gel 60), using an eluent-mix (5% NH$_4$OAc in H$_2$O:MeOH, 1:1). Free ^{64}Cu could be quantified as ^{64}Cu-EDTA complex (Rf = 0.7) by adding EDTA to the reaction mixture prior to analysis. Abbreviations: RCC, Radio chemical conversion; ^{64}Cu, copper-64.

545
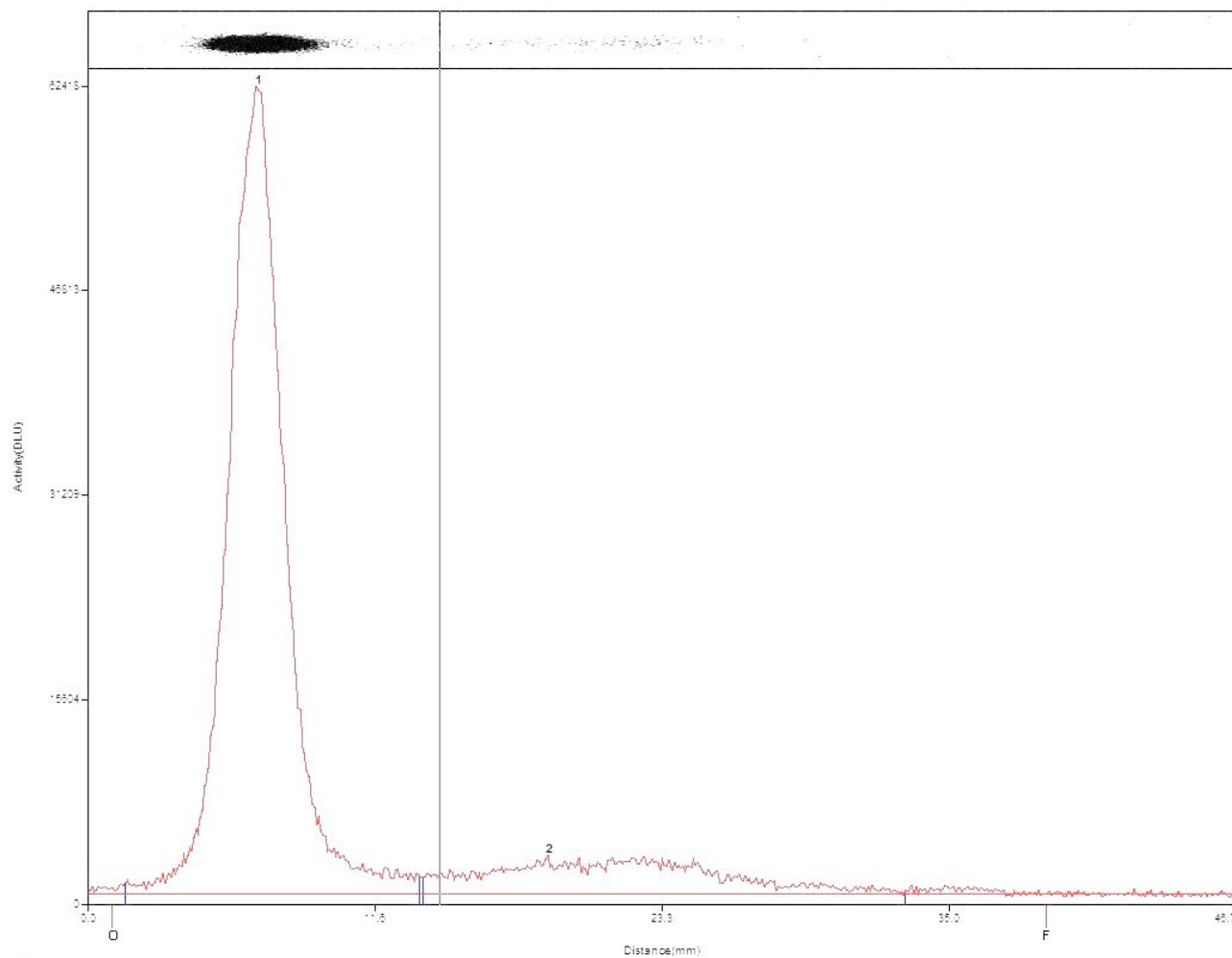
546

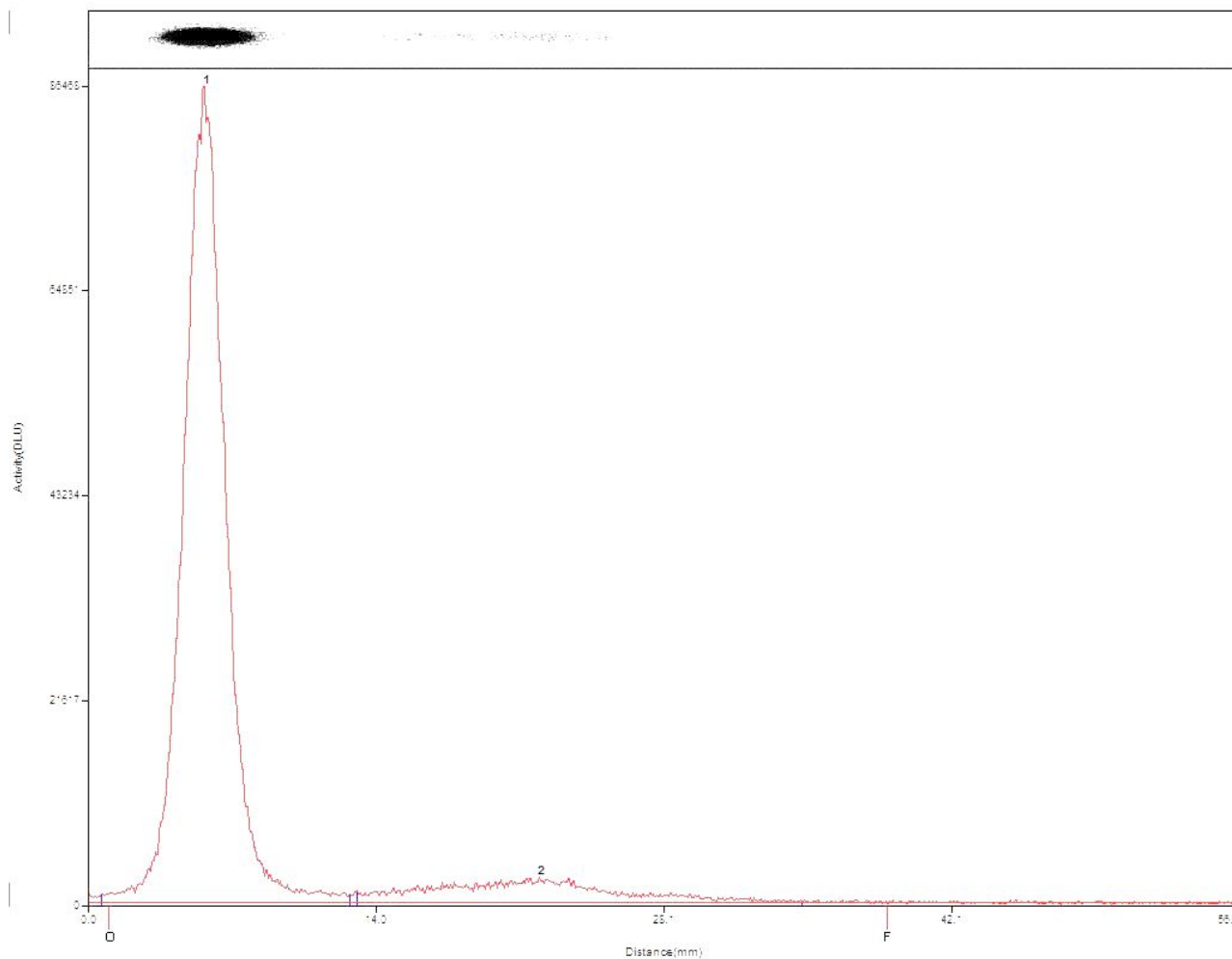547 **Fig. S8. Radio-TLC of ^{64}Cu-AuNP(40).** RCC$_3$ = 85%. The reaction was performed following the
548   general procedure, with 1.1 GBq ^{64}Cu-DOTA-TA and 0.066 mg/mL AuNPs. Radio-TLC
549   analysis was performed with a PerkinElmer Cyclone Plus phosphor imager on
550   commercially TLC pre-coated aluminum sheets (4 × 10 cm, Merck Silica gel 60), using an
551   eluent-mix (5% NH$_4$OAc in H$_2$O:MeOH, 1:1). Free ^{64}Cu could be quantified as ^{64}Cu-
552   EDTA complex (Rf = 0.7) by adding EDTA to the reaction mixture prior to analysis.
553   Abbreviations: RCC, Radio chemical conversion; ^{64}Cu, copper-64; AuNPs, gold
554   nanoparticles.
555

Fig. S9. Radio-TLC of ^{64}Cu-AuNP(8). RCC$_3$ = 89%. The reaction was performed following the general procedure, with 1.07 GBq ^{64}Cu-DOTA-TA and 0.032 mg/mL AuNPs. Radio-TLC analysis was performed with a PerkinElmer Cyclone Plus phosphor imager on commercially TLC pre-coated aluminum sheets (4 × 10 cm, Merck Silica gel 60), using an eluent-mix (5% NH$_4$OAc in H$_2$O:MeOH, 1:1). Free ^{64}Cu could be quantified as [^{64}Cu]Cu-EDTA complex (Rf = 0.7), by adding EDTA to the reaction mixture prior to analysis. Abbreviations: RCC, Radio chemical conversion; ^{64}Cu, copper-64; AuNPs, gold nanoparticles.
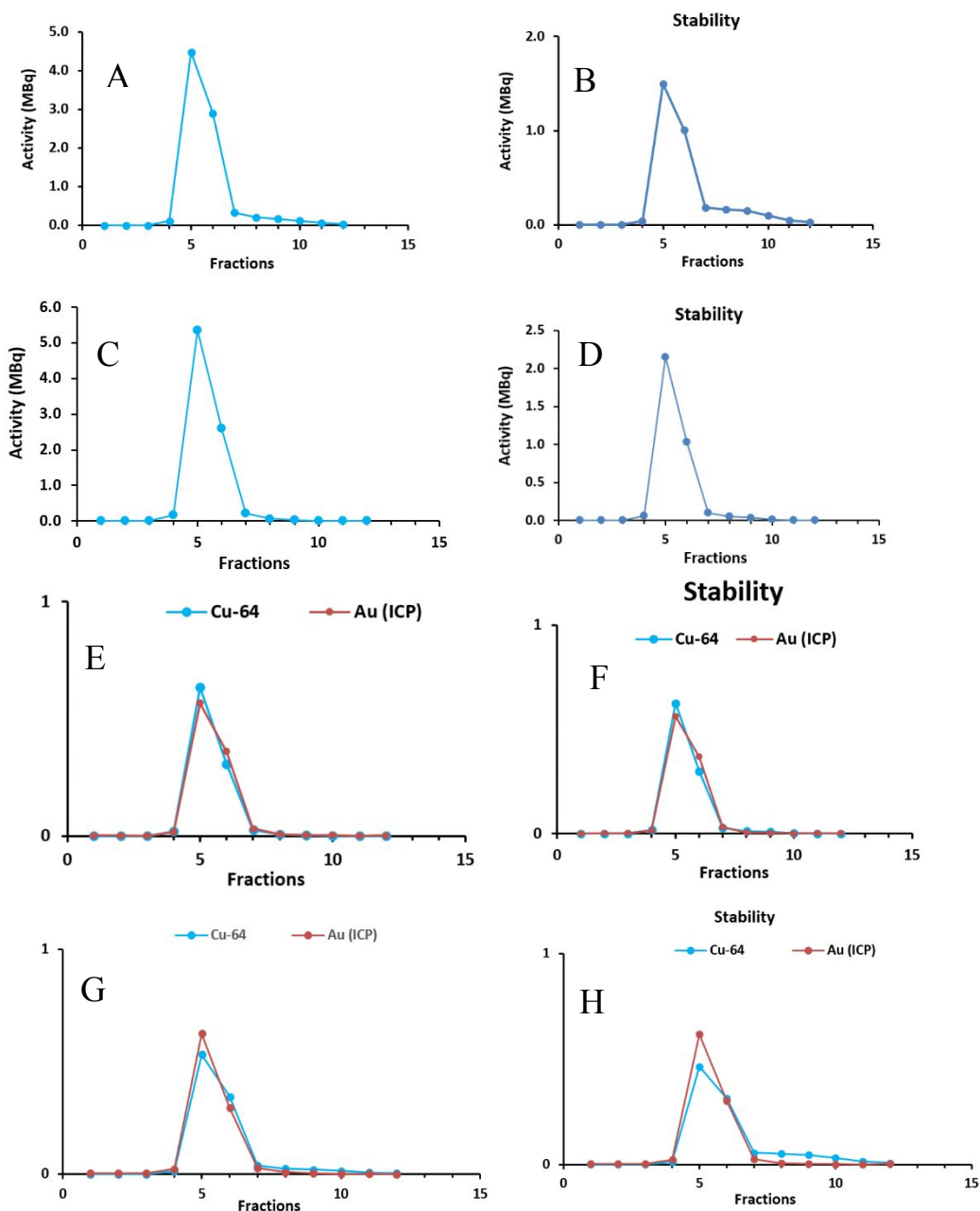
Fig. S10. Size exclusion, stability, and ICP-EOS characterization of ^{64}Cu-AuNPs. (A) ^{64}Cu-activity (MBq) analysis of ^{64}Cu-AuNPs PD-10 size exclusion fractions (Run 3). **(B)** ^{64}Cu-activity (MBq) analysis of ^{64}Cu-AuNPs PD-10 size exclusion fractions after 24 hours (stability assay for Run 3). **(C)** ^{64}Cu-activity (MBq) analysis of ^{64}Cu-AuNPs PD-10 size exclusion fractions (Run 4). **(D)** ^{64}Cu-activity (MBq) analysis of ^{64}Cu-AuNPs PD-10 size exclusion fractions after 24 hours (stability assay for Run 4). **(E)** ^{64}Cu-AuNPs ICP-OES analysis of the PD-10 size exclusion fraction, showing the overlap of ^{64}Cu activity (MBq) and ICP Au (mg/mL) for Run 3. **(F)** ^{64}Cu-AuNPs ICP-OES analysis of the PD-10 size exclusion fraction, overlap, after 24 hours (stability study for Run 3). **(G)** ^{64}Cu-AuNPs ICP-OES analysis of the PD-10 size exclusion fraction, showing the overlap of ^{64}Cu
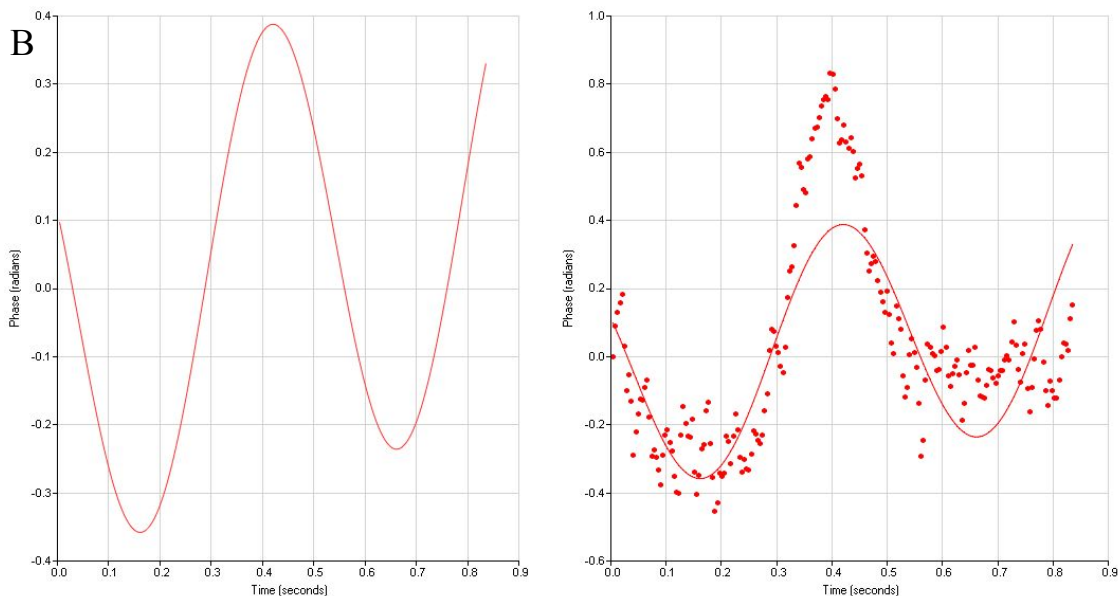
604	activity (MBq) and ICP Au (mg/mL) for Run 4. (**H**) ^{64}Cu -AuNPs ICP-OES analysis of the
605	PD-10 size exclusion fraction, overlap, after 24 hours (stability study for Run 4).
606	Abbreviations: ICP-OES, inductively coupled plasma optical emission spectroscopy; ^{64}Cu,
607	copper-64; NPs, nanoparticles; AuNPs, gold nanoparticles.

608

609
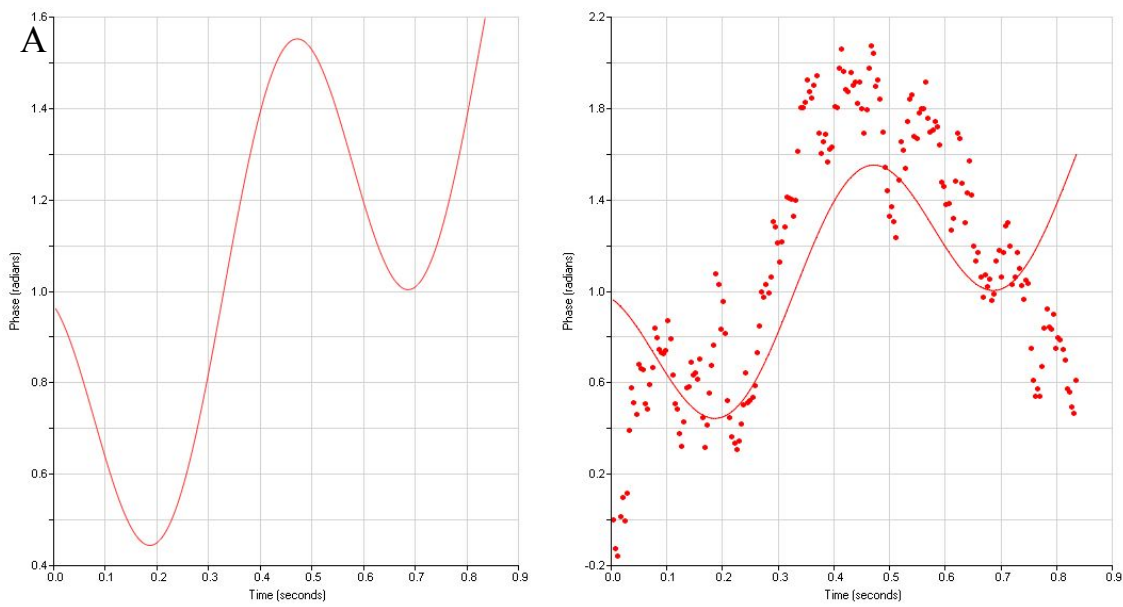
Fig. S11. Surface charge zeta potential measurements of ^{64}Cu-AuNP(40) and ^{64}Cu-AuNP(8) – Batch #3 and 4. (**A**) Batch #3: ζ = -4.86 mV ($\varnothing_{vol}$ = 40 nm), (**B**) Batch #4: ζ = -9.55 mV ($\varnothing_{vol}$ = 8 nm). Surface charge zeta-potential analysis was performed at 0.1 mg/mL NPs concentration in iso-HEPES buffer (150 mM NaCl, 10 mM HEPES, pH = 7.4) at 25 °C and was done in quintuplets. Abbreviations: NPs, nanoparticles; ζ, zeta potential; AuNPs, gold nanoparticles.

620

621

622

623
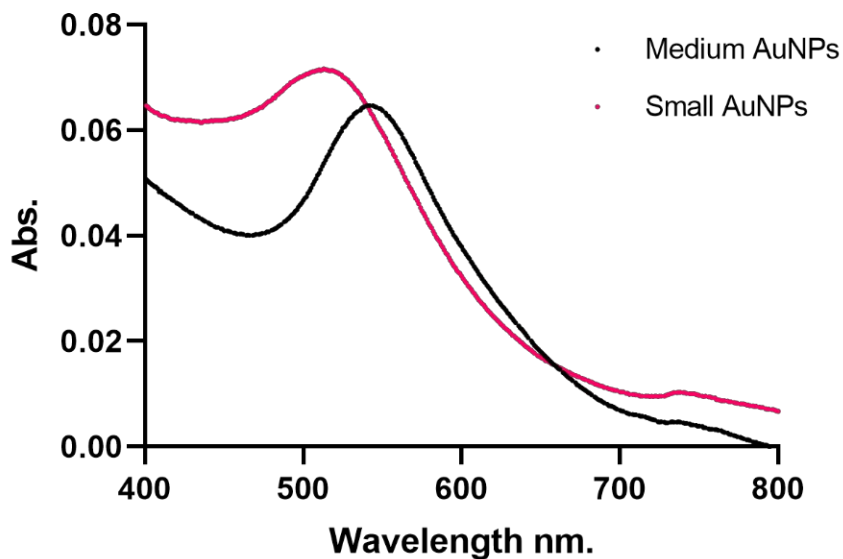
624

625

626

627

628

629

630

631

632

633

634

635

636 **Fig. S12. UV-Vis measurements of the ^{64}Cu-AuNP(40) and ^{64}Cu-AuNP(8) – Batch #3 and 4.**

637 Abbreviations: UV-Vis, ultraviolet-visible spectroscopy; Abs, absorbance; ^{64}Cu-AuNP(8),

638 small-sized gold nanoparticles with an average diameter of 8 nm; ^{64}Cu-AuNP(40),

639 medium-sized gold nanoparticles with an average diameter of 40 nm.

640

641

642

643

644

645

646

647

648
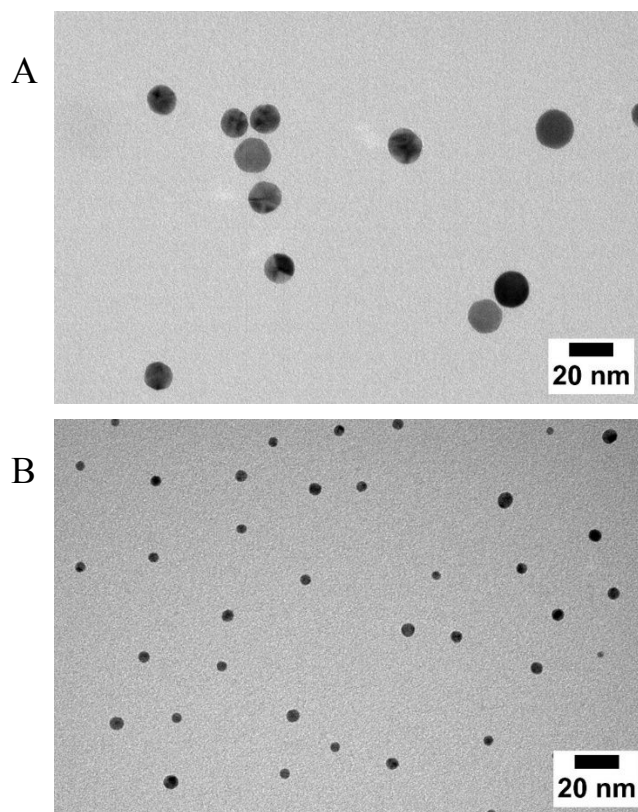
Fig. S13. TEM of the ^{64}Cu-AuNP(40) and ^{64}Cu-AuNP(8) – Batch #3 and 4. (**A**) Batch #3: $\varnothing_{TEM}$ = 14.2 ± 1.3 nm and (**B**) Batch #4: $\varnothing_{TEM}$ = 4.8 ± 0.8 nm, n = 10). Abbreviations: $\varnothing_{TEM}$, the diameter of the AuNP's gold core measured by TEM; TEM, transmission electron microscopy; ^{64}Cu-AuNP(8), radiolabeled gold nanoparticles with an average diameter of 8 nm; ^{64}Cu-AuNP(40), radiolabeled gold nanoparticles with an average diameter of 40 nm.

654
655
656
657
658
659
660
661
662
663
664
665
666
667
668
669
670
671
672
673
674
675
676
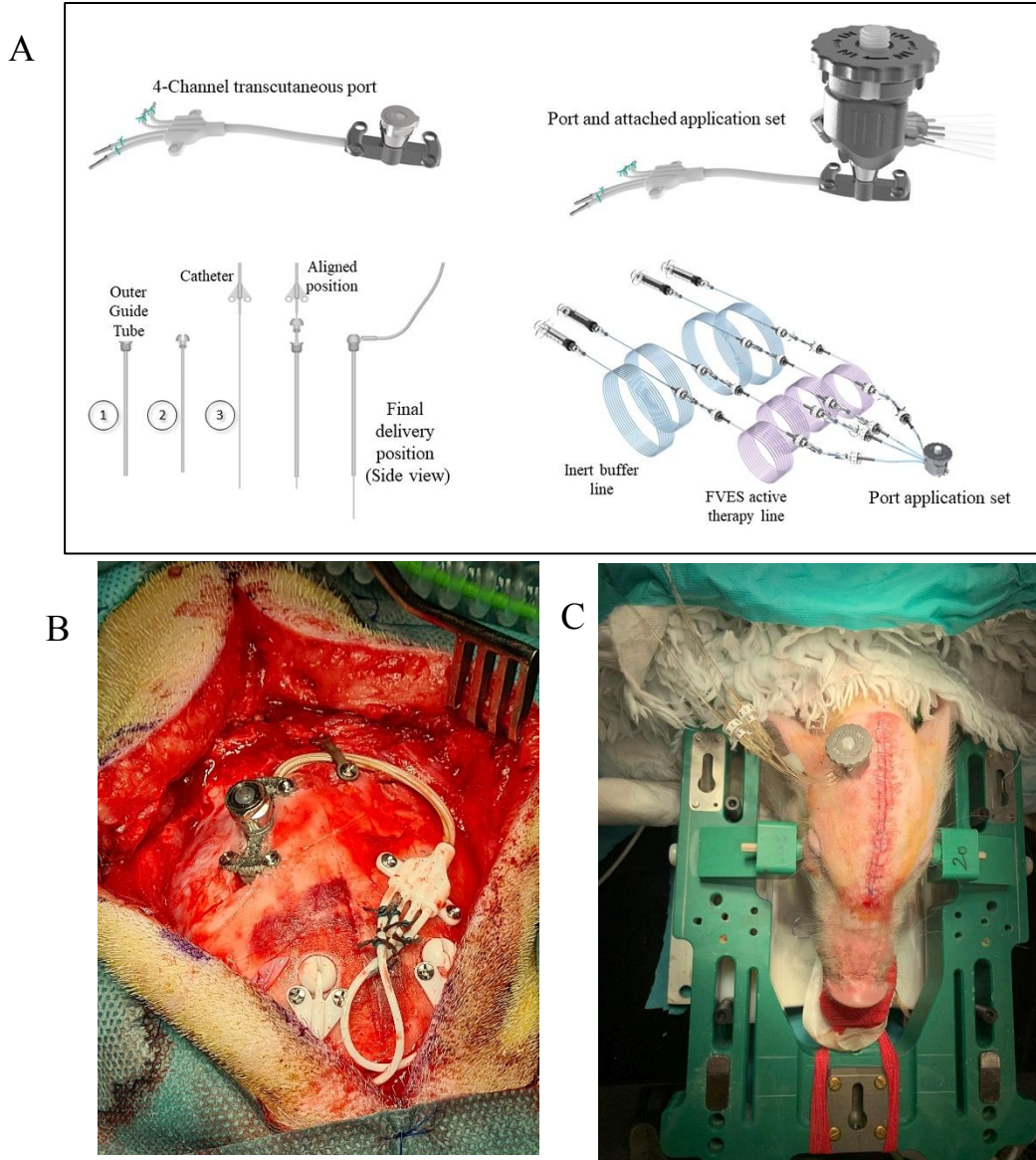
Fig. S14. neuroinfuse™ chronic drug delivery system and application setup for NPs infusions via CED. (**A**) neuroinfuse™ consisting of 3-tube 'Cut-to-any-length,' polyurethane guide-tubes and recessed step catheters, MRI compatible 4-channel titanium port, MRI compatible 4-channel application set, Fixed volume active therapy extension sets, and inert buffer infusion lines. (**B**) Implanted neuroinfuse™ 4-channel transcutaneous port (only two channels used as shown); Port manifold connected to two CED catheters, delivered through implantable recessed-step, reflux inhibiting guide tubes. (**C**) The MRI-compatible application set is attached to the reaccess port and infusion lines. Abbreviations: MRI, magnetic resonance imaging; CED, convection-enhanced delivery.
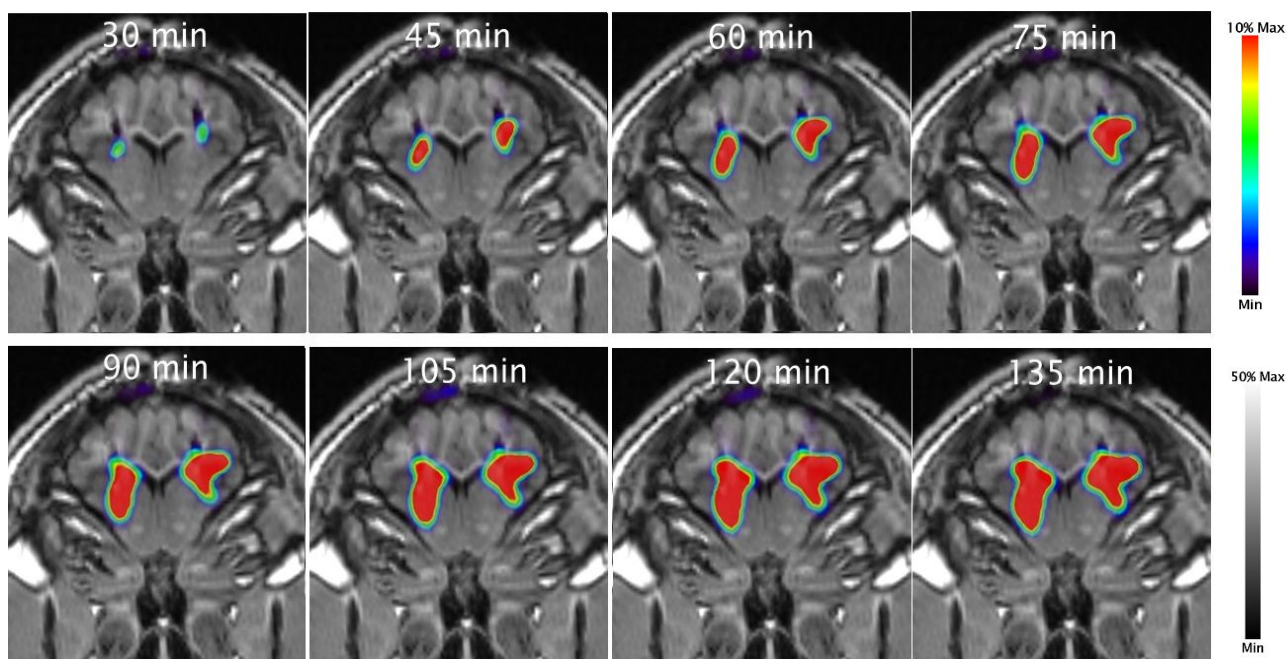
686

687
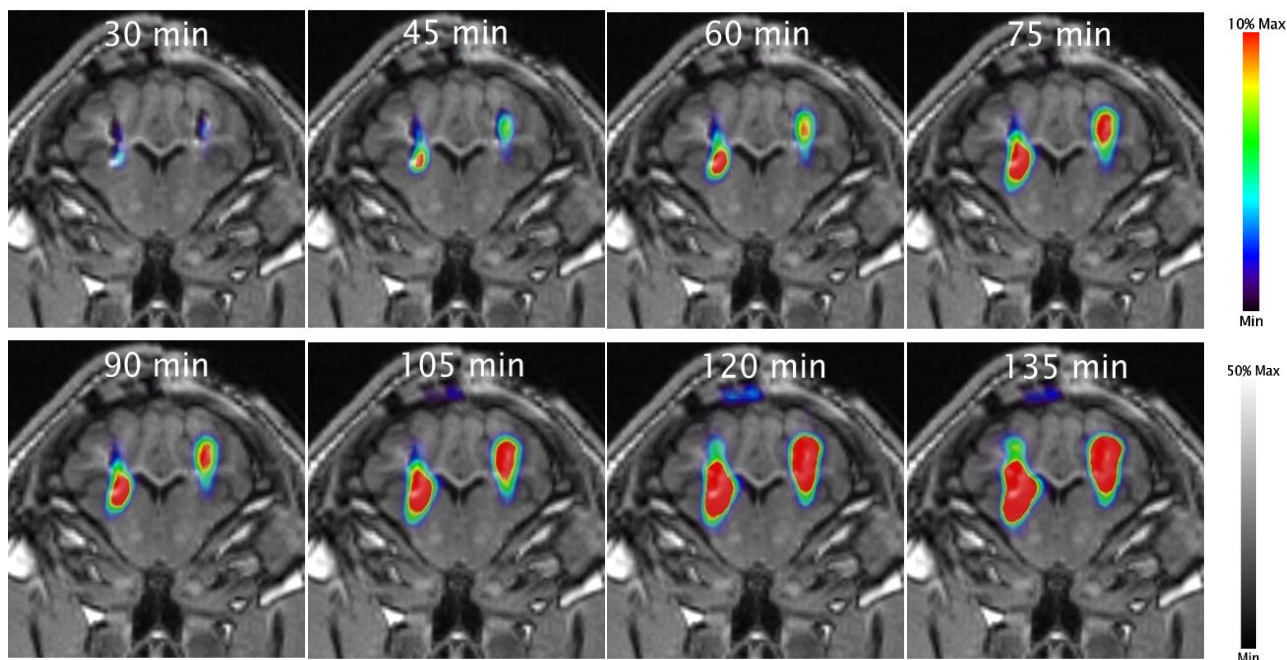
Fig. S15. Dynamic PET scans following ^{64}Cu-AuNP(40) infusion via CED. A series of dynamic PET scans from a representative minipig study was obtained at various time points following ^{64}Cu-AuNP(40) infusion into the targets. A single MRI scan was acquired at each infusion session and superimposed with the PET scans to provide anatomical guidance. The red depicts the brain region exhibiting a minimum of 10% of the maximum activity. The corresponding infusion/scan time is indicated at the top of each image. Abbreviations: PET, positron emission tomography; CED, convection-enhanced delivery; MRI, magnetic resonance imaging; ^{64}Cu-AuNP(40), radiolabeled gold nanoparticles with an average diameter of 40 nm.
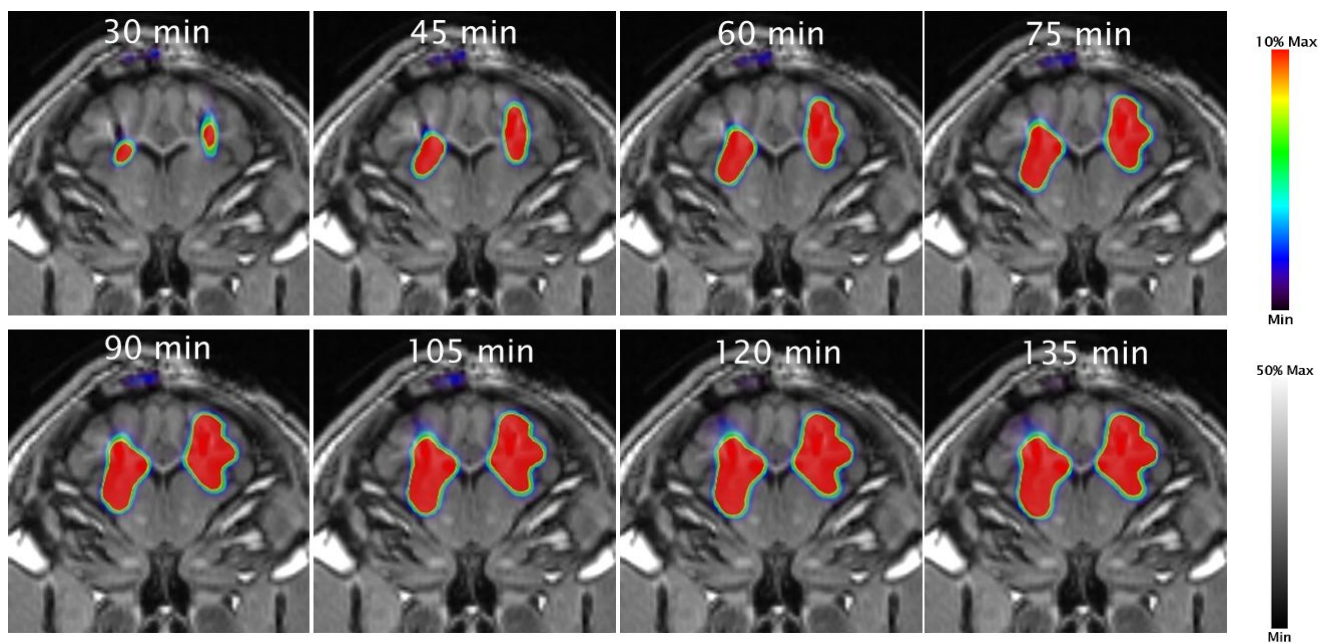
697

698
699

700

Fig. S16. Dynamic PET scans following ^{64}Cu-AuNP(8) infusion via CED. A series of dynamic PET scans from a representative minipig study obtained at various time points following ^{64}Cu-AuNP(8) infusion into the putaminal targets. A single MRI scan was acquired at each infusion session and superimposed with the PET scans to provide anatomical guidance. The red depicts the brain region exhibiting a minimum of 10% of the maximum activity. The corresponding infusion/scan time is indicated at the top of each image. Abbreviations: PET, positron emission tomography; CED, convection-enhanced delivery; MRI, magnetic resonance imaging; ^{64}Cu-AuNP(8), radiolabeled gold nanoparticles with an average diameter of 8 nm.

710

711

Fig. S17. Dynamic PET scans following ^{64}Cu-LIP(130) infusion via CED. A series of dynamic PET scans from a representative minipig study was obtained at various time points following ^{64}Cu-LIP(130) infusion into the putaminal targets. A single MRI scan was acquired at each infusion session and superimposed with the PET scans to provide anatomical guidance. The red depicts the brain region exhibiting a minimum of 10% of the maximum activity. The corresponding infusion/scan time is indicated at the top of each image. Abbreviations: PET, positron emission tomography; CED, convection-enhanced delivery; MRI, magnetic resonance imaging; ^{64}Cu-LIP(130), radiolabeled liposomes with an average diameter of 130 nm.
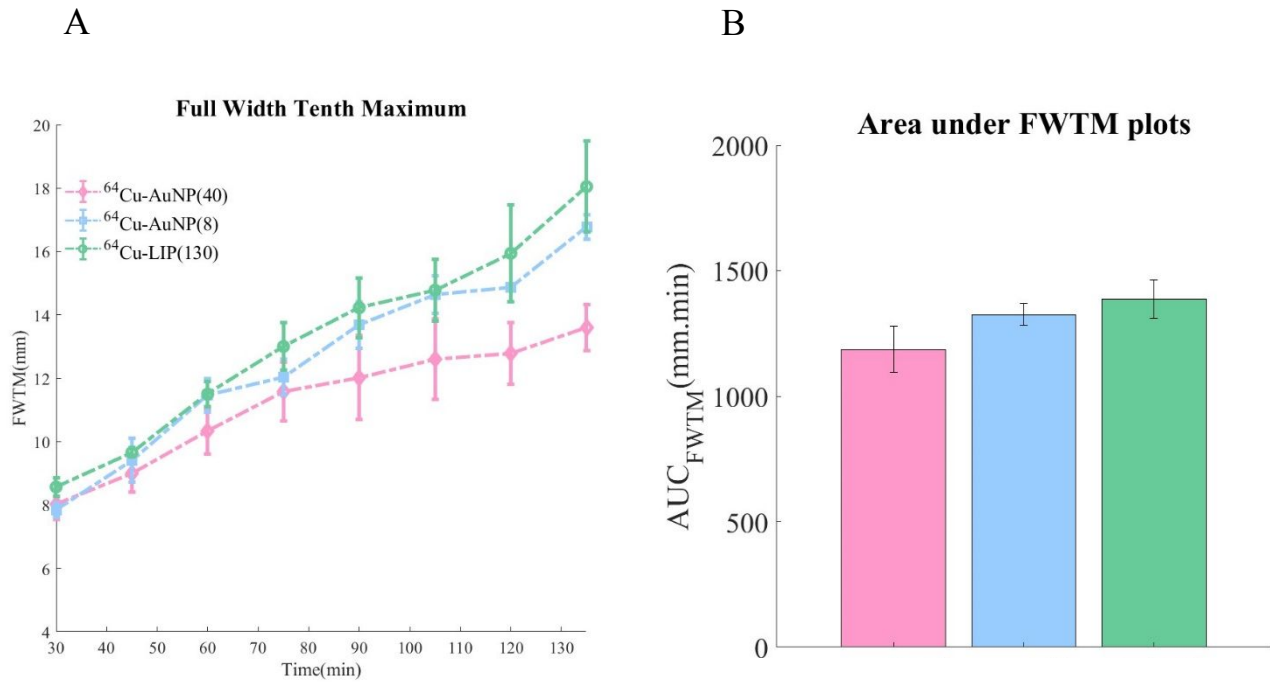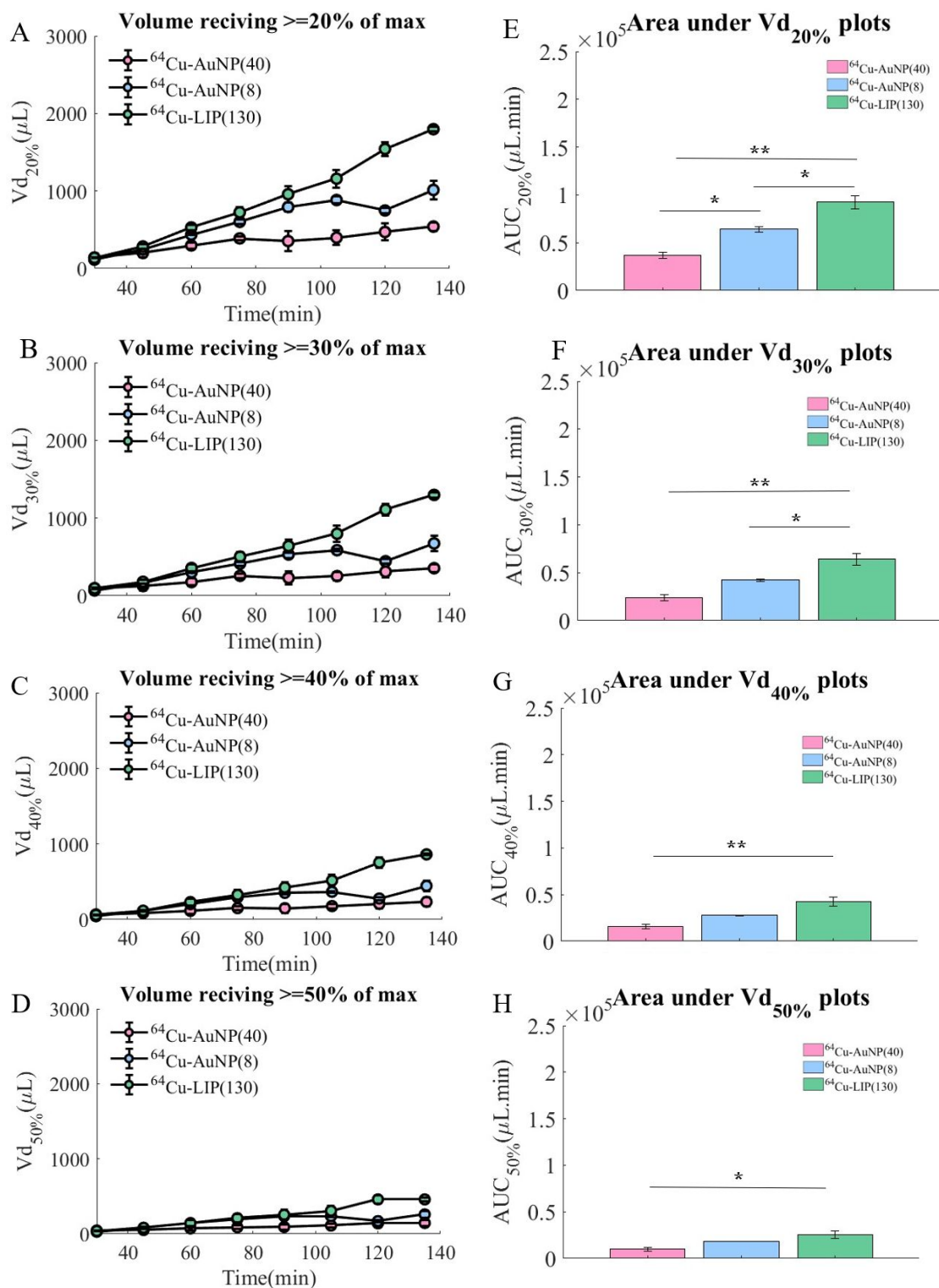
724

725

726 A   B

Full Width Tenth Maximum

Legend:
- ^{64}Cu-AuNP(40)
- ^{64}Cu-AuNP(8)
- ^{64}Cu-LIP(130)

Y-axis: FWTM(mm), from 4 to 20

X-axis: Time(min), from 30 to 130

Area under FWTM plots

Y-axis: AUC_{FWTM}(mm.min), from 0 to 2000

727

728

729 **Fig. S18. FWTM analysis and corresponding AUC plots.** (**A**) FWTM analysis of line profiles
730   crossing the center of the catheter calculated through dynamically reconstructed PET scans
731   and (**B**) corresponding AUC_{FWTM} plots. Abbreviations: PET, positron emission tomography;
732   FWTM, full-width tenth maximum; AUC_{FWTM}, the area under FWTM plots; ^{64}Cu-
733   AuNP(8), radiolabeled gold nanoparticles with an average diameter of 8 nm; ^{64}Cu-
734   AuNP(40), radiolabeled gold nanoparticles with an average diameter of 40 nm; ^{64}Cu-
735   LIP(130), radiolabeled liposomes with an average diameter of 130 nm. Data are
736   represented as mean ± standard error of the mean (n = 3-4). ANOVA followed by Tukey's
737   test was used to compare the AUC results.

738

739

Fig. S19. Multi-threshold Vd calculation and corresponding AUC analysis for different ^{64}**Cu-NPs.** (**A-D**) Dynamically assessed Vds for thresholds of 20%, 30%, 40%, and 50%, respectively. (**E-H**) corresponding AUC plots. Abbreviations: Vd, volume of distribution; AUC, area under the curve. ^{64}Cu-AuNP(8), radiolabeled gold nanoparticles with average

744   diameter of 8 nm; ^{64}Cu-AuNP(40), radiolabeled gold nanoparticles with average diameter
745   of 40 nm; ^{64}Cu-LIP(130), radiolabeled liposomes with average diameter of 130 nm. Data
746   are represented as mean ± standard error of the mean. The significant difference was *$P <$
747   0.05, **$P < 0.01$. ANOVA followed by Tukey's test was used to compare the AUC results.

748

A

B

749
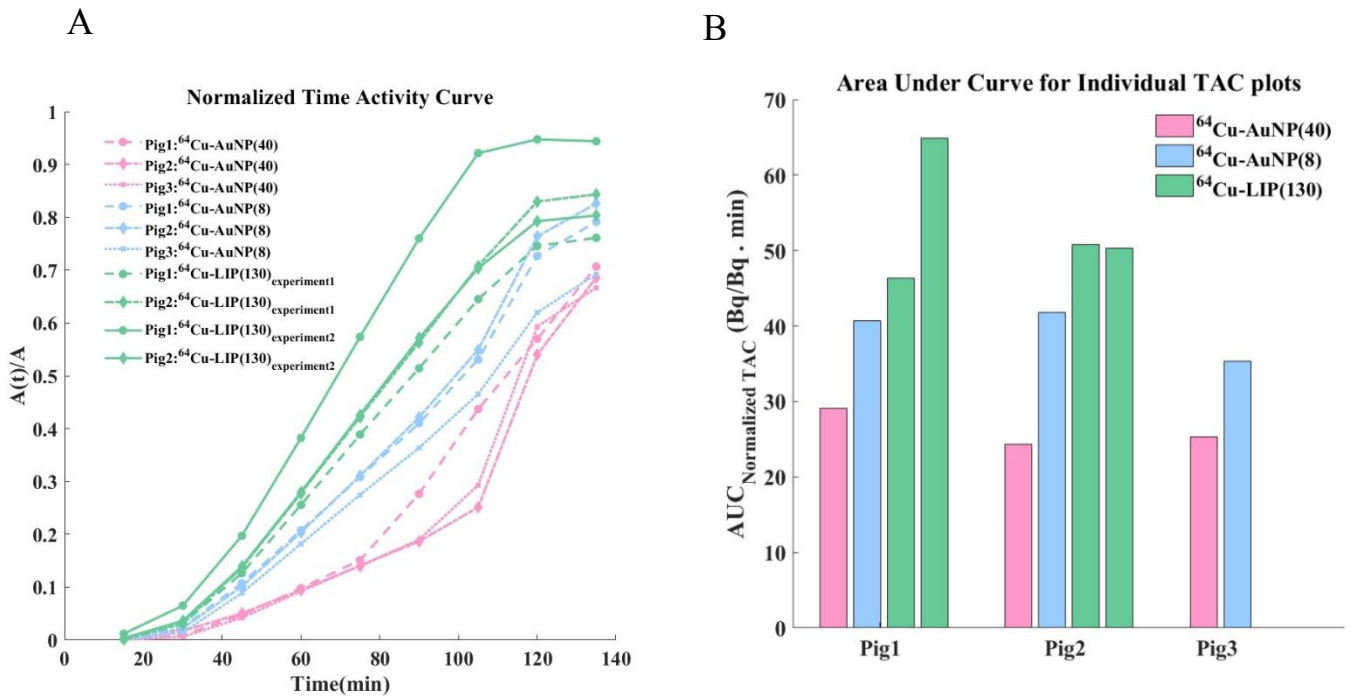
Fig. S20. Individual TAC and corresponding AUCs for different ^{64}Cu-NPs. (**A**) Individual TAC plots and (**B**) corresponding AUCs for all subjects and experiments. ^{64}Cu-AuNPs(8) and ^{64}Cu-AuNPs(40) were examined on all subjects (n = 3). However, due to a slight skin reaction near the port in one of the animals, the subject was excluded from the remainder of the study. To ensure sufficient sample size in each group of ^{64}Cu-NPs and guarantee the statistical robustness of our findings, we repeated the ^{64}Cu-LIP(130) infusion twice in the remaining subjects (n = 4). Abbreviations: TAC, time activity curve; AUC, area under curve, A(t), activity at the specific time point of t; A_{total}, total infused activity; ^{64}Cu-AuNP(8), radiolabeled gold nanoparticles with an average diameter of 8 nm; ^{64}Cu-AuNP(40), radiolabeled gold nanoparticles with an average diameter of 40 nm; ^{64}Cu-LIP(130), radiolabeled liposomes with an average diameter of 130 nm.

761

762

763

764

765

766
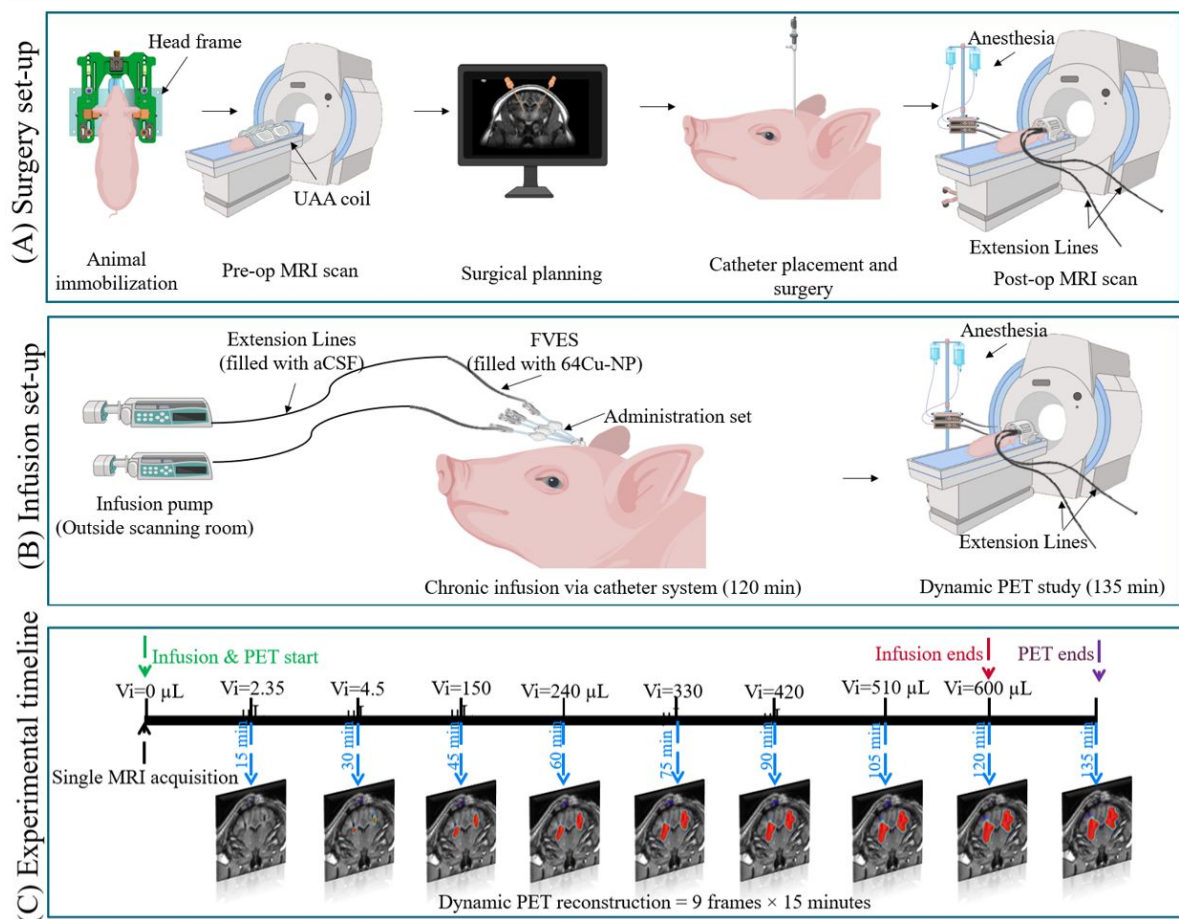
767

768

769

Fig. S21. Experimental setup and infusion procedure. (**A**) Experimental set-up on the surgery day: the anesthetized animal was immobilized in an MRI-compatible head frame, followed by surgical planning MRI scan. The MRI scan was then transferred into Neuroinspire™ software to plan the implantation trajectories of two infusion catheters within the putaminal region. A postoperative MRI was performed immediately after surgery to confirm catheter placement accuracy. (**B**) The infusion procedure for administering ^{64}Cu-NPs: 300μL FVES tubes were filled with ^{64}Cu-NPs and connected to the delivery channel in the neuroinfuse application set. After securing the infusion lines to the application set, the animal was positioned inside a head coil for PET/MRI studies. (**C**) Experimental timeline for each infusion: each infusion lasted 120 minutes, and emission data were collected over 135 minutes, beginning at the start of the infusion. Dynamic PET data was then reframed into nine frames of 15 minutes and reconstructed. MRI scan was acquired on each infusion session as an anatomical guide for PET data and quantitative analysis. Abbreviations: PET, positron emission tomography; MRI, magnetic resonance imaging; UAA, upper anterior array; ^{64}Cu-NPs, radiolabeled nanoparticles with copper-64; aCSF, artificial cerebrospinal fluid; Gd, gadolinium; V_i, volume of infusion at specific time point.

788

789

790 References

791 (1) Lilius, T. O.; Mortensen, K. N.; Deville, C.; Lohela, T. J.; Stæger, F. F.; Sigurdsson, B.;
792 Fiordaliso, E. M.; Rosenholm, M.; Kamphuis, C.; Beekman, F. J.; Jensen, A. I.; Nedergaard, M.
793 Glymphatic-Assisted Perivascular Brain Delivery of Intrathecal Small Gold Nanoparticles. *J.*
794 *Controlled Release* **2023**, *355*, 135-148. DOI: 10.1016/j.jconrel.2023.01.054.

795 (2) Sporer, E.; Poulie, C. B.; Lindegren, S.; Aneheim, E.; Jensen, H.; Bäck, T.; Kempen, P. J.;
796 Kjaer, A.; Herth, M. M.; Jensen, A. I. Surface Adsorption of the Alpha-Emitter Astatine-211 To
797 Gold Nanoparticles Is Stable In Vivo and Potentially Useful in Radionuclide Therapy. *J.*
798 *Nanotheranostics* **2021**, *2*, 196-207. DOI: 10.3390/jnt2040012.

799 (3) Mozafari, M.; Mazaheri, E.; Dormiani, K. Simple Equations Pertaining to the Particle Number
800 and Surface Area of Metallic, Polymeric, Lipidic and Vesicular Nanocarriers. *Sci. Pharm.* **2021**,
801 *89*, 15. DOI: 10.3390/scipharm89020015.

802 (4) Bienemann, A.; White, E.; Woolley, M.; Castrique, E.; Johnson, D. E.; Wyatt, M.; Murray, G.;
803 Taylor, H.; Barua, N.; Gill, S. S. The Development of an Implantable Catheter System for Chronic
804 or Intermittent Convection-Enhanced Delivery. *J. Neurosci. Methods* **2012**, *203*, 284-291. DOI:
805 10.1016/j.jneumeth.2011.10.002.

806 (5) White, E.; Woolley, M.; Bienemann, A.; Johnson, D. E.; Wyatt, M.; Murray, G.; Taylor, H.;
807 Gill, S. S. A Robust MRI-Compatible System to Facilitate Highly Accurate Stereotactic
808 Administration of Therapeutic Agents to Targets within the Brain of a Large Animal Model. *J.*
809 *Neurosci. Methods* **2011**, *195*, 78-87. DOI: 10.1016/j.jneumeth.2010.10.023.

810 (6) Barua, N. U.; Hopkins, K.; Woolley, M.; O'Sullivan, S.; Harrison, R.; Edwards, R. J.;
811 Bienemann, A. S.; Wyatt, M. J.; Arshad, A.; Gill, S. S. A Novel Implantable Catheter System with
812 Transcutaneous Port for Intermittent Convection-Enhanced Delivery of Carboplatin for Recurrent
813 Glioblastoma. *Drug delivery* **2016**, *23* (1), 167-173. DOI: 10.3109/10717544.2014.908248.

814